AD-A188 760 MODELING AND TRANSPORT IN SEMICONDUCTOR DEVICES(U) 1/1
ARIZONA STATE UNIV TEMPE D K FERRY NOV 87
ARO-21057.5-EL DAAG29-84-K-0146

UNCLASSIFIED F/G 20/12 NL

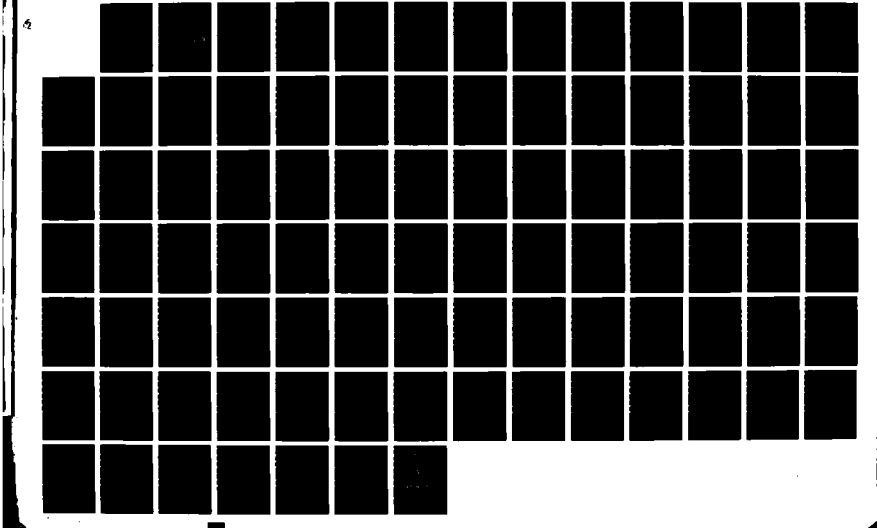

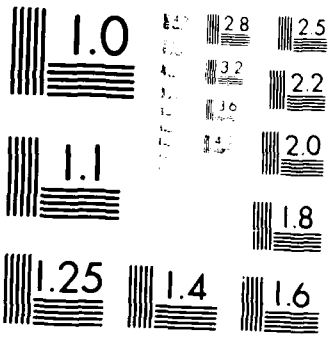

SECURITY CLASSIFICATION OF THIS PAGE (When Data Entered)

REPORT DOCUMENTATION PAGE		READ INSTRUCTIONS BEFORE COMPLETING FORM
1. REPORT NUMBER ARO 21057.5-EL	2. GOVT ACCESSION NO. N/A	3. RECIPIENT'S CATALOG NUMBER N/A
4. TITLE (and Subtitle) Modeling and Transport in Semiconductor Devices		5. TYPE OF REPORT & PERIOD COVERED 1 Sept 1984 - 31 Aug 1987 Final
		6. PERFORMING ORG. REPORT NUMBER
7. AUTHOR(s) D.K. Ferry		8. CONTRACT OR GRANT NUMBER(s) DAAG29-84-K-0146
9. PERFORMING ORGANIZATION NAME AND ADDRESS Arizona State University Tempe, AZ 85287		10. PROGRAM ELEMENT, PROJECT, TASK AREA & WORK UNIT NUMBERS
11. CONTROLLING OFFICE NAME AND ADDRESS Army Research Office Research Triangle Park, N.C. 27709		12. REPORT DATE November 1987
		13. NUMBER OF PAGES 81
14. MONITORING AGENCY NAME & ADDRESS(if different from Controlling Office)		15. SECURITY CLASS. (of this report) Unclassified
		15a. DECLASSIFICATION/DOWNGRADING SCHEDULE

16. DISTRIBUTION STATEMENT (of this Report)

Approved for public release;
Distribution unlimited.

17. DISTRIBUTION STATEMENT (of the abstract entered in Block 20, if different from Report)

NA

18. SUPPLEMENTARY NOTES

The view, opinions and/or findings contained in the report are those of the author(s) and should not be construed as an official Department of the Army position, policy, or decision, unless so designated by other documentation.

19. KEY WORDS (Continue on reverse side if necessary and identify by block number)

Laser excitation, semiconductors, hot electrons.

20. ABSTRACT (Continue on reverse side if necessary and identify by block number)

This report covers studies of picosecond laser excitation of dense electron-hole planners in semiconductors. Non-equilibrium phonons and the electron hole interaction are found to be import processes in the equilibration of the plasma.

DD FORM 1 JAN 73 1473 EDITION OF 1 NOV 65 IS OBSOLETE

SECURITY CLASSIFICATION OF THIS PAGE (When Data Entered)

ABSTRACT

The advent of time-resolved, subpicosecond laser pulse techniques has allowed us to experimentally study the ultrafast relaxation process in the far-from equilibrium electron-hole plasma in GaAs. Several theoretical studies have been carried out to explain these experimental measurements. The novel ensemble Monte Carlo simulation technique was used to investigate the cooling process of the hot laser-excited carriers, considering the roles of the carrier-phonon interaction, electron-hole interaction, and the hot phonon effects. The time-evolving distribution function, which is built self-consistently in the ensemble Monte Carlo method, has rendered it unnecessary to postulate the shape of the distribution function or to assume equal temperatures for the electrons and holes. The effects of different excitation energies and excitation levels were examined without applying external electric fields. Screening effects were investigated separately and electron-electron and hole-hole interactions were ignored in the calculations to emphasize the electron-hole interaction and hot phonon effects. Degeneracy was taken into account while the excitation level was greater than $1x10^{17}$ cm^{-3}. The study showed that the hot phonon effects do slow down the cooling rates as expected and the electron-hole interaction slows the cooling rates at low excitation levels while enhancing it at high excitation levels.

TABLE OF CONTENTS

LIST OF TABLES

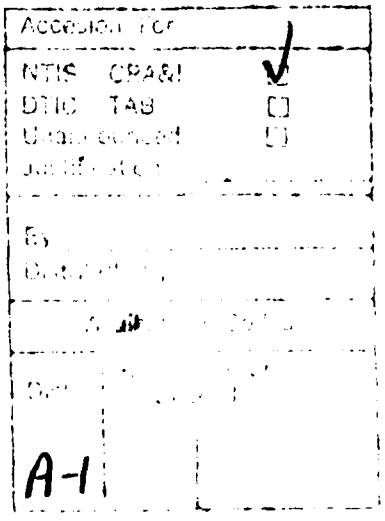

LIST OF FIGURES

CHAPTER 1

INTRODUCTION

1.1 Objective

The investigation of the ultrafast dynamics of hot photoexcited carriers in semiconductors is crucial for understanding the basic physics of scattering processes in semiconductors and has motivated many recent experimental optical studies. The processes that govern the carrier dynamics are best investigated by first generating these particles in a nonequilibrium state with a short laser pulse, and then observing their subsequent relaxation phenomenon. The study of the transient dynamics of carriers excited by subpicosecond laser pulses in GaAs has been investigated extensively in the last few years. Improvement in time resolution and sensitivity of the subpicosecond measurement system have allowed the investigation of processes such as extraction of relaxation times corresponding to different scattering processes [1], velocity overshoot of semiconductors [2,3], cooling rates of hot photoexcited carriers [4,5], lifetime of LO phonons [6-8], screening of electron-phonon interaction [9].

Several authors have carried out theoretical studies attempting to understand these measurements [11,15]. Without modern computers one had to assume a rather simple distribution function (e.g. drifted Maxwellian) and a simplified band structure in order to make the transport calculations tractable. More recently, fast computers and the development of the efficient ensemble Monte Carlo techniques have

allowed one to avoid these assumptions and use more realistic band structures without constraints on the distribution function. The objective of this thesis was to investigate an ensemble Monte Carlo technique which simulates the ultrafast relaxation processes that occur on the very short subpicosecond time regime and to evaluate the roles of electron-hole interaction and hot phonon effects on the cooling process of the hot photoexcited carriers in semiconductors.

1.2 The Approach

The important scattering mechanisms in semiconductors have been identified and the theory of these processes have been well developed in the last few years. The ensemble Monte Carlo approach developed here has taken account of the electron-phonon, hole-phonon, and electron-hole scatterings, and included the hot phonon effects in the simulation, which means the phonon system now is considered to be in a nonequilibrium state. The band structure of GaAs considered here consists of three nonparabolic valleys (Γ,L,X) in the conduction band and two parobolic heavy-hole and light-hole bands in the valence band. Since carrier-carrier scattering relies strongly on the carrier densities, the scattering mechnisms involving the weakly-populated light holes were ignored in this calculation. However, this does not mean that the light holes do not play any role in the whole cooling process. The investigation of the impact of the light holes needs further consideration. Since we assume the carriers being simulated are all generated by the laser pulse rather than from the external

doping, the elastic impurity scattering was ignored in this calculation, while the electron-electron and hole-hole scatterings also were ignored up to this stage, because of the necessity of modifying the program due to the inclusion of the hot phonon effect. This simulation has been carried out for several different excitation levels and excitation energies.

1.3 Literature Review

One of the most interesting phenomena of the hot photoexcited relaxation experiments has been the unexpectedly slow cooling of the hot distribution. It has been observed that the cooling slows as the carrier density increases [13]. The first experiment investigating the energy transfer in an optically excited electron-hole plasma was done by Höpfel, Shah, and Gossard (1986) [14]. The total energy-loss rate for electron is found to be much larger in the presence of a hole plasma due to the energy flow channelled by the electron-hole interaction which transfers energy from the hot electrons to the cold holes. The holes, after optical excitation, never obtain a temperature as high as the electrons because of the much heavier effective mass of hole and the realistic band structure of the material. Asche and Sarbei [15] estimated the electron-hole interaction and showed that the more convincing assumption of different carrier temperatures leads to a much slower cooling rate than obtained for equal carrier temperatures [16]. Although the assumption of equal carrier temperatures in Pötz's approach is not very reasonable from a physical point of view,

the demonstration of the influence of the reabsorption of the non-equilibrium phonons still has to be taken into account.

In the present study, a strongly perturbed phonon distribution is found in the first picosecond after the laser pulse. This is responsible for a reduction of the cooling rate of the laser-excited carriers. Inclusion of the hot phonon effects, and the screening of the electron-phonon interaction, has led to a very close agreement between the theory and experiment for laser-excited GaAs. The calculations using a random phase approximation screening model [17] and static Debye-Hückel screening model [18,21] all showed that the cooling slows significantly due to screening. An analytical 2T model including the hot phonon effect for the cooling of hot photoexcited carriers in GaAs was proposed by Pötz [19] recently. Several other analytical studies of nonequilibrium phonons have appeared in the literature [16,20-24].

CHAPTER 2

THEORETICAL BACKGROUND

2.1 Band Structure of GaAs

The band structure of a crystalline solid, i.e. the energy-momentum (E-k) relationship, is generally obtained by solving the Schrodinger equation of an approximate one-electron problem. Quite often, the band structure is very complicated and can only be calculated semi-empirically utilizing a computer. A variety of numerical methods have been used to theoretically calculated the energy bands of solids. The methods used most often for semiconductors are the orthogonalized plane-wave method [10], the pseudopotential method [26], and $\vec{k} \cdot \vec{p}$ method [27]. Figure 2.1 shows the calculated band structure of GaAs, including the spin-orbit interaction [28]. Fig. 2.2 illustrates the important region of the GaAs band structure in transport. The top of the valence band at k=0, the Γ point, is degenerate with the upper valence band, termed the heavy-hole band, the lower valence band, termed the light-hole band. About 0.34 ev [29] below the Γ point lies the spin-orbit split-off band. The minimum of the conduction band also lies at k=0, which makes GaAs a direct-gap semiconductor material, in contrast to Si. The energy gap E_g of GaAs is temperature-dependent and considered to be 1.51 ev for $T \leq 77°K$, 1.439 ev for $T > 77°K$ here.

As shown in Fig. 2.2, the valence band can be approximately fitted by two parabolic bands with different curvatures: a wider band

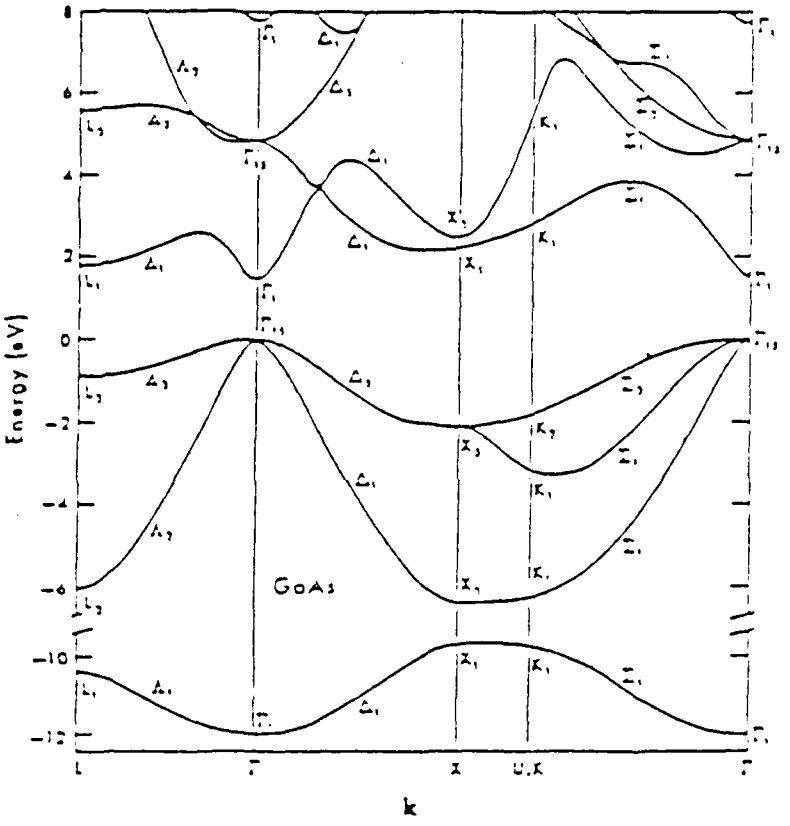

Fig. 2.1 Energy band structure of GaAs

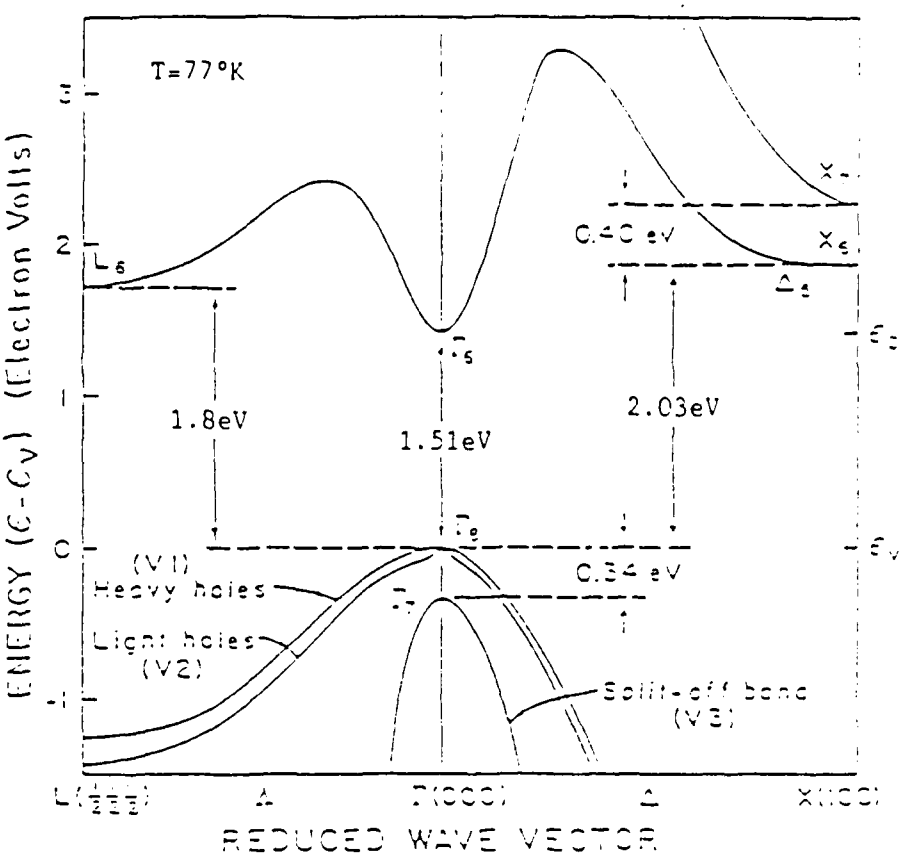

Fig. 2.2 Schematic representation of the energy band structure of GaAs in [100] and [111] directions in the vicinity of the band edge.

with smaller $\frac{\partial^2 E}{\partial^2 k}$ (the heavy-hole band) and the narrower band with larger $\frac{\partial^2 E}{\partial^2 k}$ (the light-hole band). The effective mass of the carriers is generally a tensor quantity with components m^*_{ij} defined as $m^*_{ij} = \left(\frac{1}{\hbar^2} \frac{\partial^2 E}{\partial^2 k} \right)^{-1}$. In reality, these two bands are warped and nonparabolic as a result of their degeneracy and the interaction among the bands. The reason we treat the valence band as parabolic is that at the present time one can get analytical expressions for the carrier-carrier scatterings only for parabolic bands. There are two sets of satellite conduction-band valleys in GaAs. The L-valleys have minima at the boundary of the Brillouin zone in the (111) directions at an energy about 0.30 ev [30,31] above the central valley. The X-valleys have minima at zone edges in the (100) directions at an energy about 0.50 ev [32] above the central valley. Due to the tunability of lasers, we can control the excitation energy to determine whether or not excitation of the electrons up to the satellite valleys is occurring. These three valleys are nonparabolic and anisotropic, each requiring a longitudinal and transverse mass component to describe it.

The E-k relationship for a nonparabolic band takes the form [12]

$$\frac{\hbar^2 k^2}{2m} = E(1+\alpha E),$$

and

$$\alpha = \frac{1}{E_g}\left(1 - \frac{m^*}{m_c}\right).$$

where α is the nonparabolicity factor. For a parabolic warped band, the E-k relationship becomes [37]

$$E(k) = \frac{\hbar^2 k^2}{2m} g(\theta, \phi),$$

where

$$g(\theta, \phi) = A \pm \left[B^2 + \frac{C^2}{k^4}\left(k_x^2 k_y^2 + k_x^2 k_z^2 + k_y^2 k_z^2\right) \right]^{1/2}.$$

The average effective mass for such a band is given by

$$\frac{1}{m_{av}} = \frac{1}{m_o}\left[A \pm \left(B^2 + \frac{C^2}{6}\right)\right],$$

where the positive and negative signs are for the light-hole and heavy-hole respectively. For GaAs, A=-6.98, B=-4.5, and C=6.2 [33].

2.2 Scattering Mechanisms

The scattering processes that are included in calculating the time-evolved carrier distributions on a subpicosecond time scale can be classified into two groups [34]: processes in which the scattering rates are independent of carrier concentrations, such as unscreened carrier-phonon scattering, and processes in which the scattering rates depend strongly on carrier densities, such as carrier-carrier scattering. In general, the carrier-density-dependent processes

consist of the screening effect of the carrier-phonon scattering and the carrier-carrier scattering, while the carrier-density-independent processes including the acoustic phonon scattering, polar optical phonon scattering, non-equivalent intervalley phonon scattering, and equivalent intervalley phonon scattering. The carrier-carrier scattering can be classified as inter- and intra-valley electron-electron scatterings, inter- and intra-band hole-hole scatterings, and electron-hole scattering. Since the Coulomb cross section decreases rapidly as momentum transfer increases, the scatterings caused by ionized impurities or other carriers are generally considered only for intravalley or intraband transitions [35].

According to time-dependent first-order perturbation theory, the transition probability per unit time for scattering from a state $\vec{k}$ to a state $\vec{k}'$ due to a perturbing hamiltonian H' is given by the Fermi-Golden rule

$$S(\vec{k},\vec{k}') = \frac{2\pi}{\hbar}|\langle\vec{k}|H'|\vec{k}'\rangle|\,\delta(E-E'),$$

where E and E' are the eigenenergies of the initial and final states respectively. It is convenient to use Fourier transformation to interpret H', which gives the squared matrix element the following form [36,37]:

$$|\langle\vec{k}|H'|\vec{k}'\rangle|^2 = V(\vec{q})G(\vec{k},\vec{k}'),$$

thus the transition probability is

$$S(\vec{k},\vec{k}') = \frac{2\pi}{\hbar}V(\vec{q})G(\vec{k},\vec{k}')\delta(E-E'),$$

where $V(\vec{q})$ contains the dependence on $\Delta\vec{k}$ of the squared Fourier transformation of the interaction potential and $G(\vec{k},\vec{k}')$ represents the overlap integral

$$G(\vec{k},\vec{k}') = \left| \int_{cell} u^{*}_{\vec{k}'}(\vec{r}) u_{\vec{k}}(\vec{r}) d\vec{r} \right|^2.$$

The overlap factor equals unity for parabolic bands, while it is less than unity if nonparabolicity is significant. The overlap effect was ignored for electrons because $G(\vec{k},\vec{k}')$ in this case is very close to unity. The overlap factor was taken to be 0.5 for holes [52] in the calculations. Actually, for the intraband transition of holes, the overlap factor is taken as [48]

$$G(\vec{k},\vec{k}') = \frac{1}{4}\left(1+3\cos^2\theta\right),$$

and for interband transitions,

$$G(\vec{k},\vec{k}') = \frac{3}{4}\sin^2\theta,$$

where θ is the angle between $\vec{k}$ and $\vec{k}'$. The various scattering processes considered in this calculation will be discussed individually in the following two sections. The scattering probabilities per unit time with respect to the carrier's energy are well formulated for each scattering mechanism.

2.2.1 Formulations of Electron Scattering Rates

Acoustic Phonon Scattering

This scattering process involves the electrons being scattered by intravalley acoustic phonons through deformation potential interaction which is due directly to the strain caused by the acoustic waves in the crystals. The energy involved is small, thus we can treat it as being approximately elastic in nature. The squared matrix element [37] is given as

$$V_{ac}(q) = \frac{\Xi_1^2 \hbar q}{2\rho u}\left(N_q + \frac{1}{2} \pm \frac{1}{2}\right),$$

$$N_q = \frac{1}{\exp\left(\frac{\hbar u q}{k_B T}\right) - 1},$$

where Ξ_1 is the acoustic deformation potential, ρ the crystal density, q the phonon wave-vector, u the speed of sound, N_q the Bose-Einstein distribution function, and the $\pm$ signs represent the absorption and emission respectively. Since we are not interested in a lattice temperature above 300 $^{\circ}$K, scattering processes involving more than one phonon are neglected. According to the elastic, equipartition-energy approximation, the scattering rate for nonparabolic bands is given as [35]

$$P_{e,ac}(E) = \frac{(2m^*)^{3/2} k_B T \Xi_1^2}{2\pi\rho u^2 \hbar^4} E^{\frac{1}{2}} (1+\alpha E)^{\frac{1}{2}} (1+2\alpha E).$$

The angles of the final wave-vector can be determined by random numbers r_1 and r_2 because this process completely randomizes the momentum, and

$$\cos\theta = 1-2r_1, \tag{2.1}$$

$$\phi = 2\pi r_2. \tag{2.2}$$

Polar Optical Phonon Scattering

In polar semiconductors such as GaAs, the polarization of the crystal, arising from the vibrations of the longitudinal optical branch, results in an additional interaction with the carriers termed the polar optical interaction. The energy of polar optical phonons in intravalley transitions can be assumed constant, given by $\hbar\omega_o = k_B T_{op}$, where T_{op} is the equivalent temperature of the phonons. The polar optical scattering due to TO phonons is negligible in contrast to LO phonons. The squared matrix element is [37]

$$V_{po}(q) = \frac{2\pi e^2 \hbar\omega_o}{q^2} \left(\frac{1}{\varepsilon_\infty} - \frac{1}{\varepsilon_o}\right) \left(N_o + \frac{1}{2} \mp \frac{1}{2}\right),$$

where ω_o is the longitudinal optical mode frequency, and ε_∞, ε_o the dielectric constants for infinite and zero frequencies respectively.

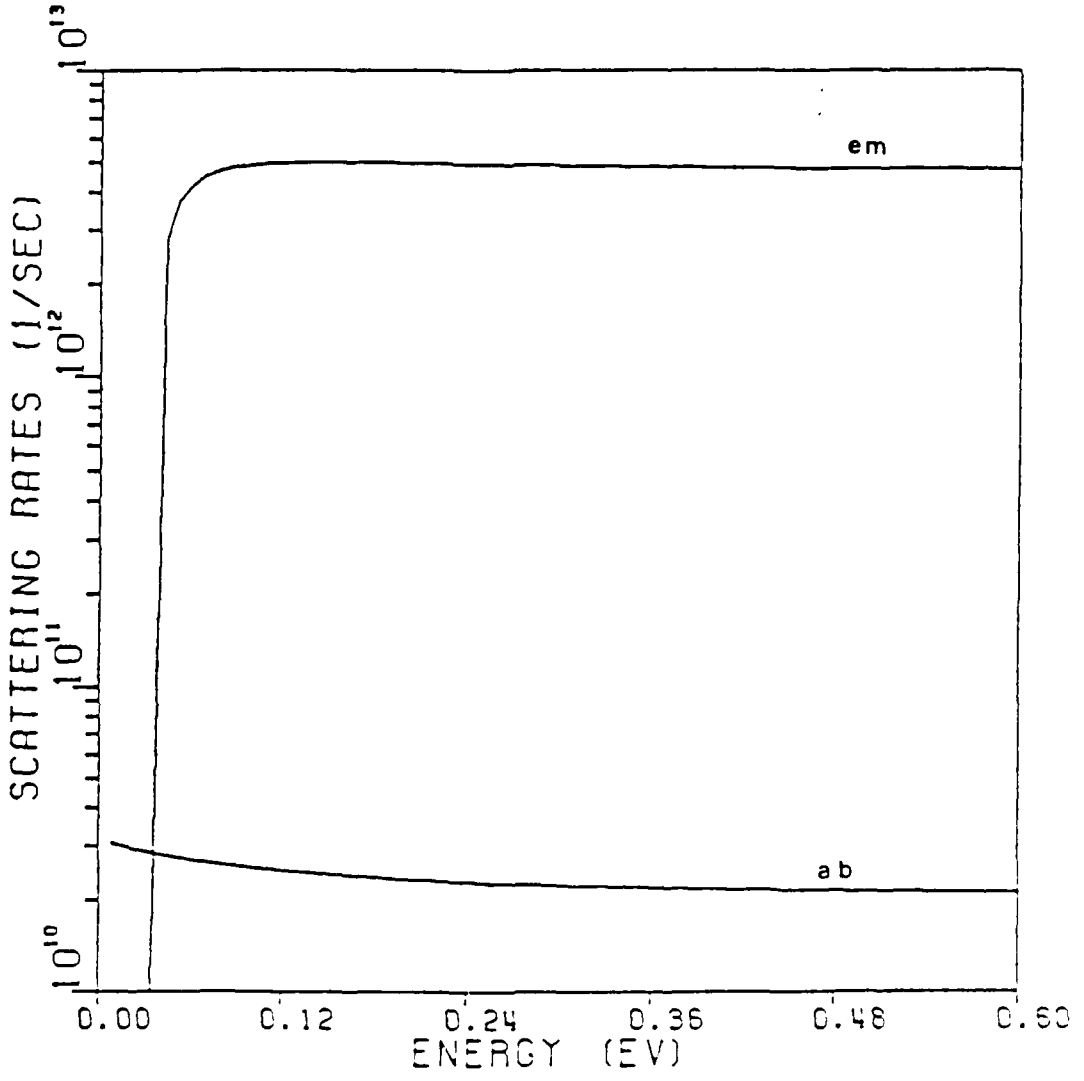

Fig. 2.3 Energy dependence of the polar optical scattering rate for the Γ valley of GaAs at 77K.

N_o becomes q-independent and has the form

$$N_o = \frac{1}{\exp\left(\frac{\hbar\omega_o}{k_B T}\right) - 1},$$

where T is the lattice temperature. The scattering probability per unit time is given as [12]

$$P_{e,op}(E) = \frac{em^{*1/2}\omega_o}{\sqrt{2}\hbar}\left(\frac{1}{\varepsilon_\infty} - \frac{1}{\varepsilon_o}\right)\frac{1+2\alpha E'}{\sqrt{\gamma(E)}}F_o(E,E')\left(N_o+\frac{1}{2}\pm\frac{1}{2}\right),$$

where $E' = E \pm \hbar\omega_o$, $\gamma(E) = E(1+\alpha E)$, and

$$F_o(E,E') = \ln\left(\frac{\sqrt{\gamma(E)} + \sqrt{\gamma(E')}}{\sqrt{\gamma(E)} - \sqrt{\gamma(E')}}\right).$$

The total scattering rate for polar optical scattering decreases as energy increases as shown in Fig. 2.3. This scattering is strongly anisotropic and the angular dependence of the scattering is given by [36]

$$P(\theta)d\theta = \frac{\sin\theta d\theta}{\gamma(E)+\gamma(E')-2\sqrt{\gamma(E)\gamma(E')}\cos\theta}.$$

Using random numbers r and r_1 uniformly distributed between 0 and 1, we get

$$\cos\theta = \left[(1+f)-(1+2f)^r\right]/f,$$

$$\phi = 2\pi r_1,$$

where

$$f = \frac{2\sqrt{\gamma(E)\gamma(E')}}{\left[\sqrt{\gamma(E)}-\sqrt{\gamma(E')}\right]^2}.$$

Equivalent Intervalley Phonon Scattering

This scattering process is always treated similarly to intravalley scattering by optical phonons via the deformation potential interaction [49,50]. The polar and piezoelectric interactions are always neglected for intervalley phonon scattering because the large momentum transfer involved diminishes its probability to occur. The energy of the phonon involved is also treated as a constant as in the case of intravalley optical phonon scattering, given by $\hbar\omega_i$. The squared matrix element is [37]

$$V(q) = \frac{D_i^2\hbar^2}{2\rho\hbar\omega_i}\left(N_q+\frac{1}{2}\mp\frac{1}{2}\right),$$

where D_i is the deformation potential and ω_i is the intervalley phonon frequency. The resulting scattering rate is [35]

$$P_{e,ei}(E) = (Z-1)\frac{m^{*3/2}D_i^2}{\sqrt{2}\pi\rho\hbar^2(\hbar\omega_i)}\sqrt{\gamma(E')}(1+2\alpha E')\left(N_i+\frac{1}{2}\mp\frac{1}{2}\right).$$

$$E' = E \pm \hbar\omega_i,$$

where Z is the number of equivalent final valleys, and N_i is the population of the phonons involved in the transitions. All states in the energy-conserving sphere are equally probable to be the final state after scattering.

Non-equivalent Intervalley Phonon Scattering

This scattering mechanism is responsible for negative differential mobility as the origin of the velocity overshoot phenomenon observed in GaAs. Electrons transfer between the central valley and one of the outer satellite valleys either by absorption or emission of a phonon. The squared matrix element is given as [37]

$$V(q) = \frac{D_{ij}^2 \hbar^2}{2\rho\hbar\omega_{ij}}\left(N_q + \frac{1}{2} \pm \frac{1}{2}\right),$$

where D_{ij} is the deformation potential for scattering from ith valley to jth valley induced by a phonon of energy $\hbar\omega_{ij}$. The scattering rate is given as [35]

$$P_{e,ni}(E) = (Z-1)\frac{m^{*3/2} D_{ij}^2}{\sqrt{2}\pi\rho\hbar^2(\hbar\omega_{ij})}\sqrt{\gamma(E')}(1+2\alpha_j E')\left(N_{ij} + \frac{1}{2} \pm \frac{1}{2}\right),$$

$$E' = E \pm \hbar\omega_{ij} - \Delta\xi_{ji}.$$

where α_j is the nonparabolicity factor of the jth valley, and $\Delta\xi_{ji}$ is the energy difference between the bottoms of the initial and final valleys. Since the intervalley scattering randomizes the momentum, there is no preferred direction for the final state. These rates are shown in Figs. 2.4 and 2.5.

Electron-Hole Scattering

At high carrier densities, the collisions of the carriers with each other need to be considered. The electrons and holes are assumed to interact among themselves via a screened Coulomb potential

$$V(r) = \frac{e^2}{4\pi\varepsilon r}\exp(-\beta r),$$

where ε is the dielectric constant of the material and β is the inverse screening length which can be calculated self-consistently in the ensemble Monte Carlo method. According to the Fermi-Golden rule, the transition probability for two carriers to transit from state $(\vec{k}_1,\vec{k}_2)$ to state $(\vec{k}_1',\vec{k}_2')$ due to the coulomb interaction is

$$S_{\vec{k}_1,\vec{k}_2\rightarrow\vec{k}_1',\vec{k}_2'} = \frac{2\pi}{\hbar}|M|^2 f_{\vec{k}_1} f_{\vec{k}_2}\left(1-f_{\vec{k}_1'}\right)\left(1-f_{\vec{k}_2'}\right)\delta\left(E_{\vec{k}_1'}+E_{\vec{k}_2'}-E_{\vec{k}_1}-E_{\vec{k}_2}\right),$$

where $f_{\vec{k}}$ and $E_{\vec{k}}$ are the occupation probability and the energy at state $\vec{k}$ respectively. The matrix element is given as [36]

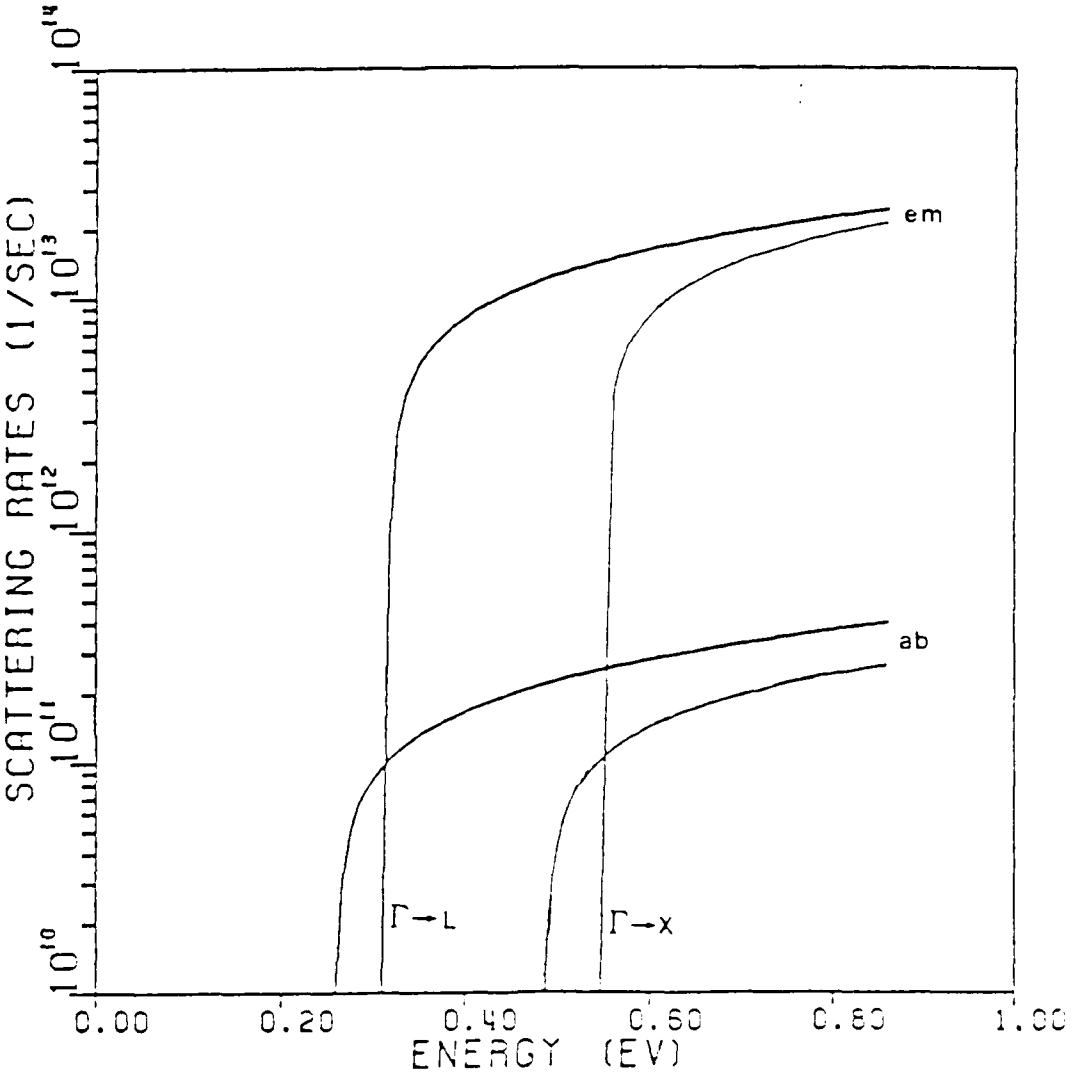

Fig. 2.4 Energy dependence of the intervalley scattering rate for the Γ valley of GaAs at 77K.

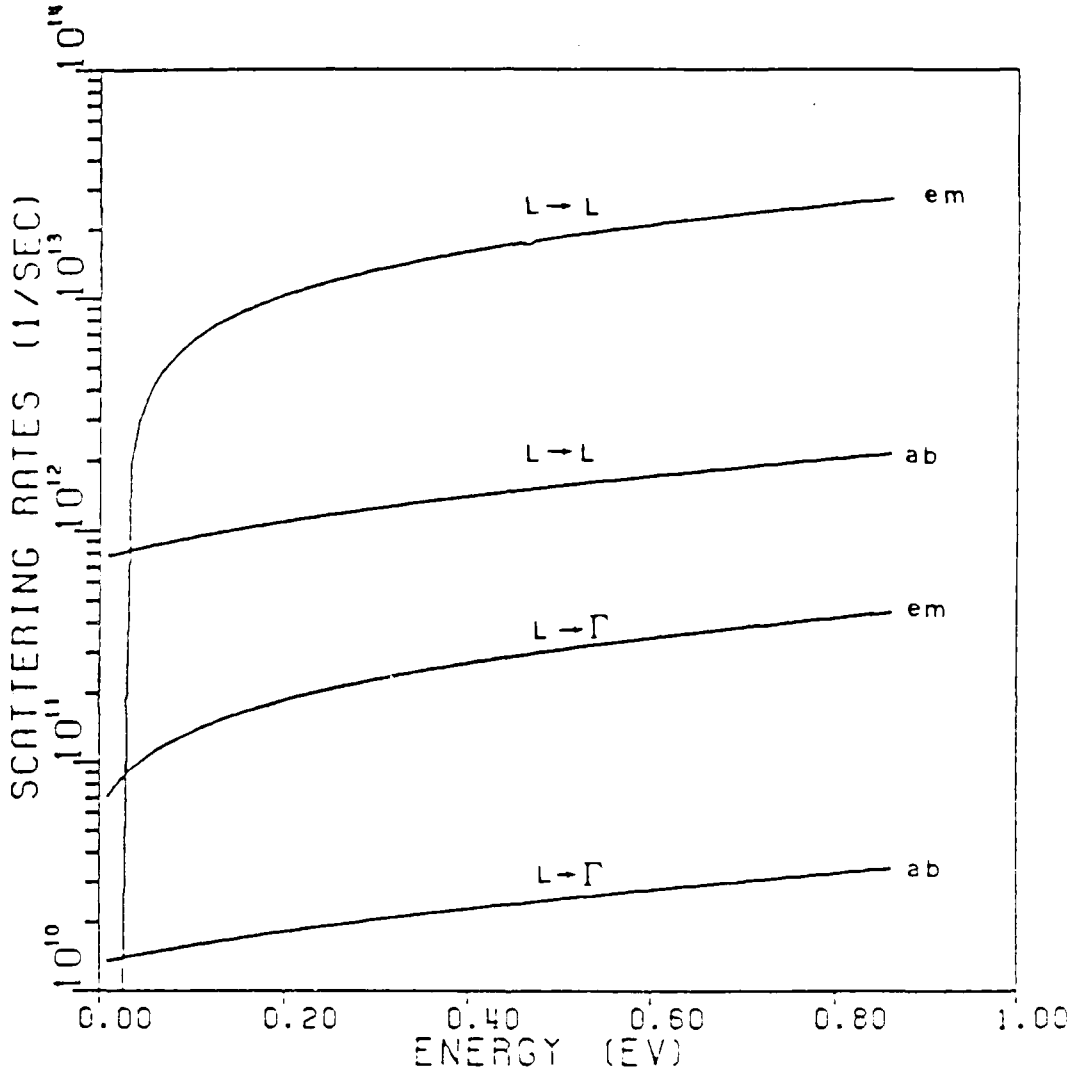

Fig. 2.5 Energy dependence of the equivalent (L→L) and non-equivalent intervalley (L→Γ) scattering rate in the L valley of GaAs at 77K.

$$M = \langle \vec{k}_1, \vec{k}_2 | V(r) | \vec{k}_1', \vec{k}_2' \rangle = \frac{e^2}{\varepsilon} \frac{\delta_{\vec{k}_1+\vec{k}_2, \vec{k}_1'+\vec{k}_2'}}{|\vec{k}_1'-\vec{k}_1|^2+\beta^2},$$

where the initial and final states are considered to be plane waves. The scattering rate of the carrier-carrier scattering is obtained by summing $S_{\vec{k}_1,\vec{k}_2 \to \vec{k}_1',\vec{k}_2'}$ over $\vec{k}_2$, $\vec{k}_2'$ and $\vec{k}_1'$. Since the final state degeneracy is considered separately in the EMC method [51], all the final states are assumed to be unoccupied, so that, we can set $f_{\vec{k}_1'} = f_{\vec{k}_2'} = 0$, and $f_{\vec{k}_1} = 1$. Under these conditions, the scattering rate for an electron in state $|\vec{k}_1\rangle$ scattered by a hole in state $|\vec{k}_2\rangle$ is given as [36]

$$\Gamma_{eh}(\vec{k}_1) = \frac{2\pi}{\hbar} \sum_{\vec{k}_2} \sum_{\vec{k}_1'} \sum_{\vec{k}_2'} \left(\frac{e^2}{\varepsilon}\right)^2 f_{\vec{k}_2} \frac{\delta_{\vec{k}_1+\vec{k}_2, \vec{k}_1'+\vec{k}_2'}}{\left[|\vec{k}_1'-\vec{k}_1|^2+\beta^2\right]^2} \delta\left(E_{\vec{k}_1'} + E_{\vec{k}_2'} - E_{\vec{k}_1} - E_{\vec{k}_2}\right).$$

After special manipulations (for the details, see Ref.[36]), $P_{eh}(\vec{k}_1)$ can be expressed as

$$P_{eh}(\vec{k}_1) = \frac{\mu e^4}{2\pi\hbar^3\varepsilon^2} \sum_{\vec{k}_2} f_{k_2} \frac{g}{\beta^2\left(g^2+\beta^2\right)}, \tag{2.3}$$

where the relative wave vector $\vec{g}$ and reduced mass μ are defined as

$$\vec{g} = 2\mu\left(\frac{\vec{k}_1}{m_e} - \frac{\vec{k}_2}{m_h}\right),$$

and

$$\mu = \frac{m_e m_h}{m_e + m_h}.$$

Rewriting (2.3) in integral form, we obtain

$$P_{eh}(\vec{k}_1) = \frac{p\mu e^4}{2\pi\varepsilon^2 h^3} \int d^3\vec{k}_2 f_h(\vec{k}_2) \frac{Q_{eh}}{\beta^2 \left(Q_{eh}^2 + \beta^2\right)}, \qquad (2.4)$$

where $Q_{eh} = 2\mu \left| \frac{\vec{k}_1}{m_e} - \frac{\vec{k}_2}{m_h} \right|$, and p is the concentration of holes. Equation (2.4) is now used by replacing the distribution function integral by a particle sum in the Monte Carlo procedure.

2.2.2 Formulations of Hole Scattering Rates

A parabolic and spherically symmetric two-band model is considered when calculating the scattering rates for holes. The third split-off band is omitted. In the valence band, the polar optical and deformation potential scatterings dominate while the impurity scattering is neglected in this calculation.

Acoustic Phonon Scattering

The acoustic-phonon coupling constant Ξ_u is given as [52]

$$\Xi_1^2 = \left[\frac{1}{3} + \frac{2}{3}\left(\frac{s_t}{s_l}\right)^2\right]\left[a^2 + \frac{c_l}{c_t}\left(b^2 + \frac{1}{2}d^2\right)\right],$$

where s_l, s_t are the longitudinal and transverse sound velocities, a, b and d are the deformation potential constants [52]. The average longitudinal and transverse elastic constants c_l and c_t are given as

$$c_l = \frac{1}{5}\left(3c_{11}+2c_{12}+4c_{44} \right),$$

$$c_t = \frac{1}{5}\left(c_{11}-c_{12}+3c_{44} \right),$$

where c_{11}, c_{12} and c_{44} are the crystal elastic constants. The values of all the parameters used in the calculations are shown in Table 2.1 [53]. The resulting scattering rate for intraband transitions is given as [52]

$$P_{ii}(E) = \frac{\Xi_1^2 k_B T (2m_i)^{3/2}}{4\rho \bar{s}^2 \pi \hbar^4} E^{1/2} G_{ii},$$

where $\bar{s}$ is given by

$$\bar{s}^2 = \frac{1}{3}s_l^2 + \frac{2}{3}s_t^2.$$

For interband transitions, we have

$$P_{ij}(E) = P_{jj}(E)\left(\frac{m_j}{m_i}\right)^{1/2}, \qquad (i \neq j)$$

Bulk material parameters		
Crystal elastic constants (dyn/cm^2):	C_{11}	11.88×10^{11}
	C_{12}	5.38×10^{11}
	C_{44}	5.49×10^{11}
[100] longitudinal sound velocity S_l (cm/sec)		4.73×10^5
[100] transverse sound velocity S_t (cm/sec)		3.34×10^5
Scattering-rate parameters		
Effective masses: heavy-hole band	m_{hh}	$0.45 m_o$
light-hole band	m_{lh}	$0.082 m_o$
Optical-phonon energy (eV)		0.036
Deformation-potential constants (eV):	a	6.7
	b	1.7
	d	4.4

Table 2.1 Parameters for GaAs hole-transport program.

where G_{ij} result from the integration of $G(\theta)$ over all scattering angles θ, and it is found $G_{11} = G_{22} = G_{12} = G_{21} = 0.5$.

Non-Polar Optical Phonon Scattering

The scattering rate for intraband processes is given by [36]

$$P_{ii}(E) = \frac{(2m_i)^{3/2} D_o^2}{4\pi\rho\hbar^3\omega_o}\left(E \pm \hbar\omega_o\right)^{1/2}\left(N_o + \frac{1}{2} \pm \frac{1}{2}\right)G_{ii},$$

while for interband transitions, it becomes

$$P_{ij}(E) = \frac{(2m_i)^{3/2} D_o^2}{4\pi\rho\hbar^3\omega_o}\left(E \pm \hbar\omega_o\right)^{1/2}\left(N_o + \frac{1}{2} \pm \frac{1}{2}\right)G_{ij}.$$

The angles of the final wave-vector after scattering can be chosen by (2.1) and (2.2) because this scattering process completely randomizes the momentum. These rates are shown in Figs. 2.6 and 2.7.

Polar Optical Phonon Scattering

The scattering rate for intraband transitions is [36]

$$P_{ii}(E) = \frac{B_{po} m_i}{2\pi\hbar^2}\left(2m_i\right)^{-1/2} E^{-1/2}\left(N_o + \frac{1}{2} \pm \frac{1}{2}\right)G_{ii}(E)\Psi_i(E),$$

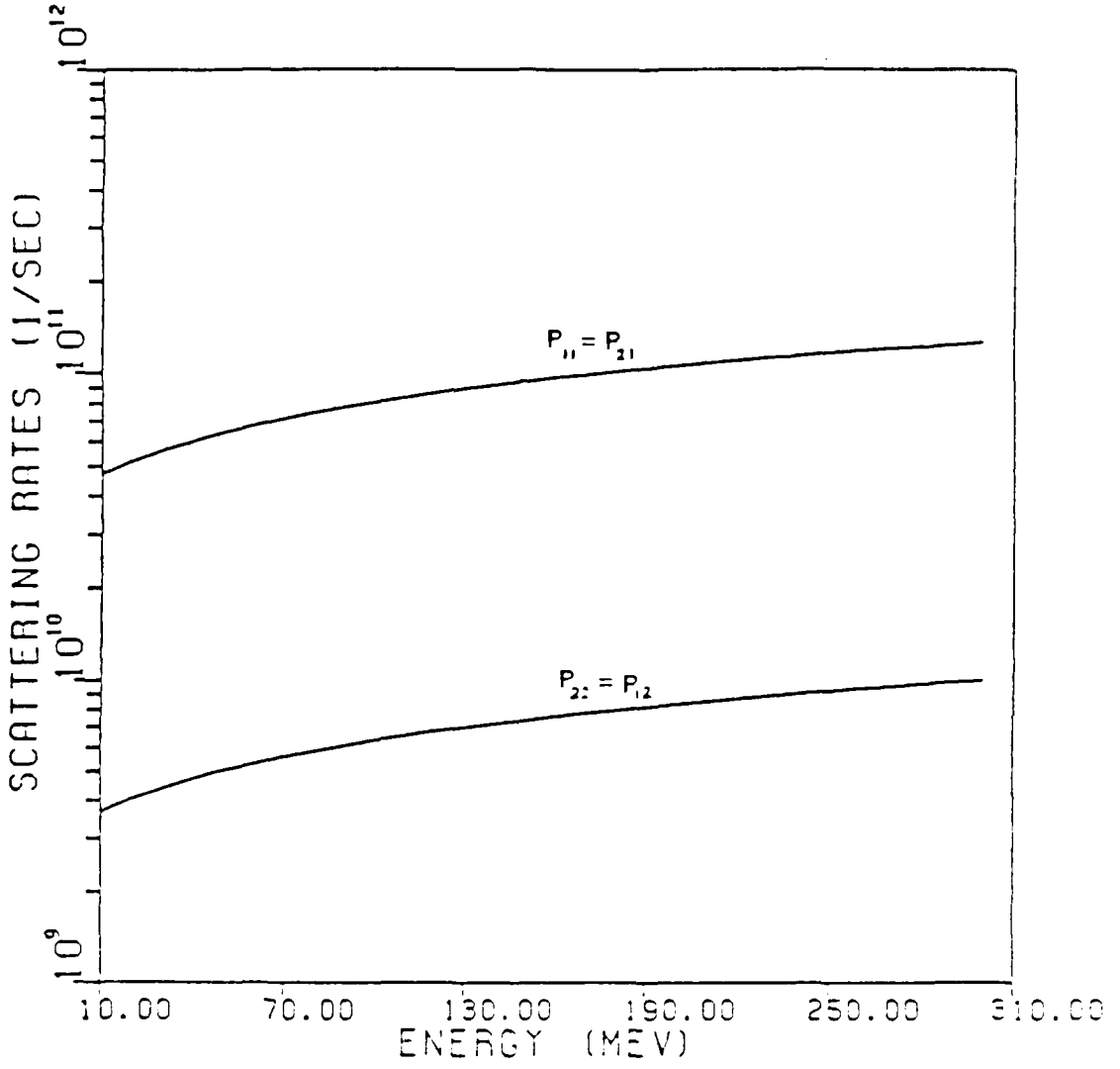

Fig. 2.6 Energy dependence of deformation potential absorption rates for holes in GaAs at 77K.

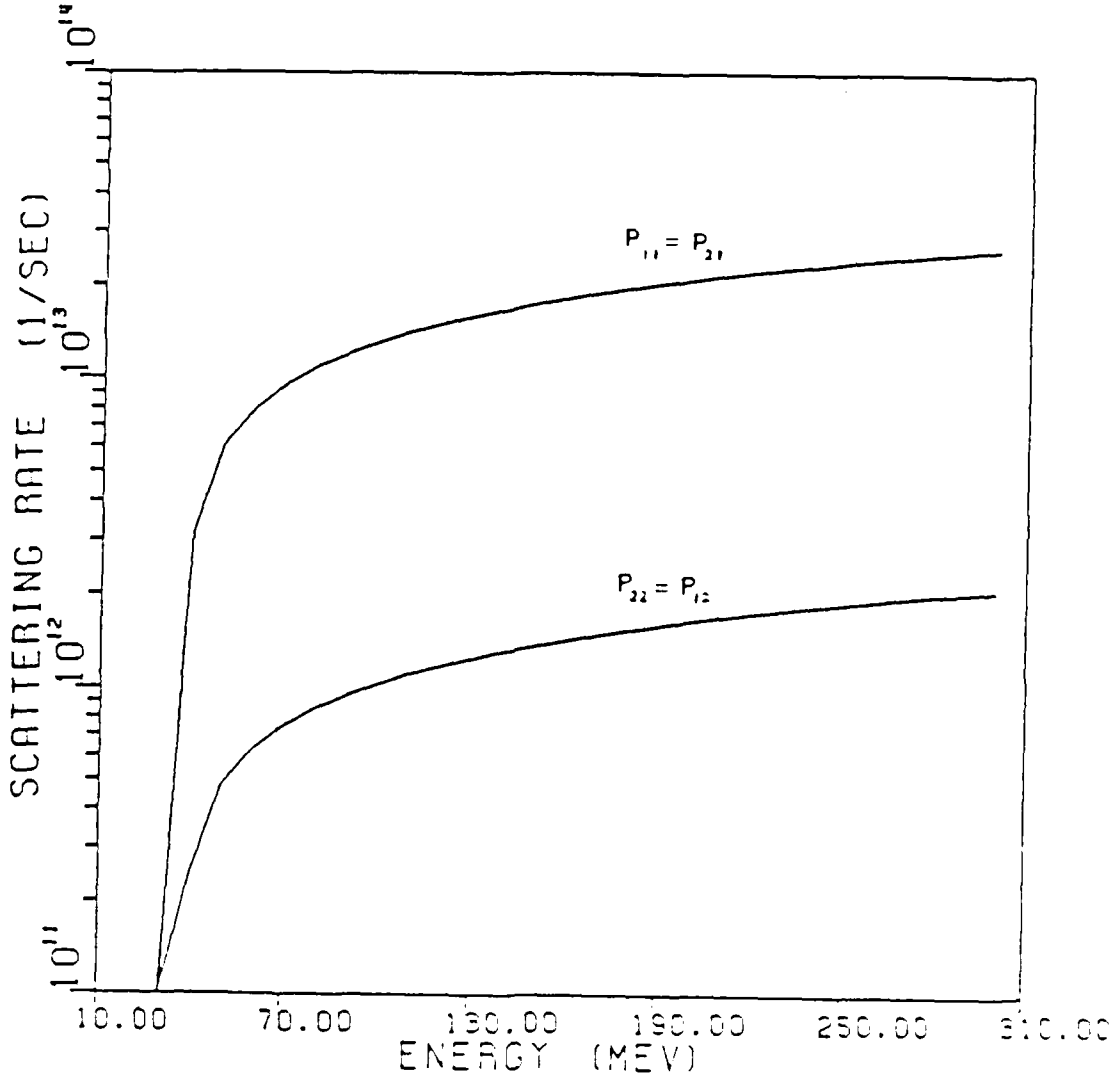

Fig. 2.7 Energy dependence of deformation potential emission rates for holes in GaAs at 77K.

where

$$G_{ii}(E) = \frac{1}{4}\left\{1 + 3\Phi_i(E)\left[\Phi_i(E) - \frac{1}{\Psi_i(E)}\right]\right\},$$

$$\Psi_i(E) = \ln\left|\frac{\sqrt{E}+\sqrt{E'}}{\sqrt{E}-\sqrt{E'}}\right|,$$

$$\Phi_i(E) = \frac{E+E'}{2\sqrt{EE'}},$$

$$N_o = \frac{1}{\exp\left(\frac{\hbar\omega_o}{k_B T}\right) - 1},$$

and $E' = E \pm \hbar\omega_o$. For interband transitions, this becomes

$$P_{ij}(E) = \frac{B_{po} m_j}{2\pi\hbar^2}\left(2m_i\right)^{-1/2} E^{-1/2}\left(N_o + \frac{1}{2} \pm \frac{1}{2}\right) G_{ij}(E)\Psi_{ij}(E),$$

where

$$G_{ij}(E) = \frac{3}{2}\left\{1 - \Phi_{ij}(E)\left[\Phi_{ij}(E) - \frac{1}{\Psi_{ij}(E)}\right]\right\},$$

$$\Psi_{ij}(E) = \ln\left|\frac{\sqrt{E} + \sqrt{\frac{m_i}{m_j}E'}}{\sqrt{E} - \sqrt{\frac{m_i}{m_j}E'}}\right|.$$

$$\Phi_{ij}(E) = \frac{E + \frac{m_j}{m_i}E'}{2\sqrt{\frac{m_j}{m_i}EE'}}.$$

The angular dependence for intraband transitions is

$$P_{ii}(\theta)d\theta \sim \frac{(1+3\cos^2\theta)\sin\theta d\theta}{k^2+k'^2-2kk'\cos\theta},$$

while for interband transitions, it becomes

$$P_{ij}(\theta)d\theta \sim \frac{(1-\cos^2\theta)\sin\theta d\theta}{k^2+k'^2-2kk'\cos\theta}.$$

These scattering rates are plotted in Figs. 2.8 and 2.9.

Hole-Electron Scattering

The scattering rate for an hole in state $|\vec{k}_1\rangle$ scattered by an electron in state $|\vec{k}_2\rangle$ is given as [36]

$$P_{he}(\vec{k}_1) = \frac{n_e e^4}{2\pi\varepsilon^2\hbar^3}\int d^3\vec{k}_2 f_e(\vec{k}_2)\frac{Q_{he}}{\beta^2\left(Q_{he}^2+\beta^2\right)}, \qquad (2.5)$$

where

$$Q_{he} = 2\mu\left|\frac{\vec{k}_1}{m_h} - \frac{\vec{k}_2}{m_e}\right|.$$

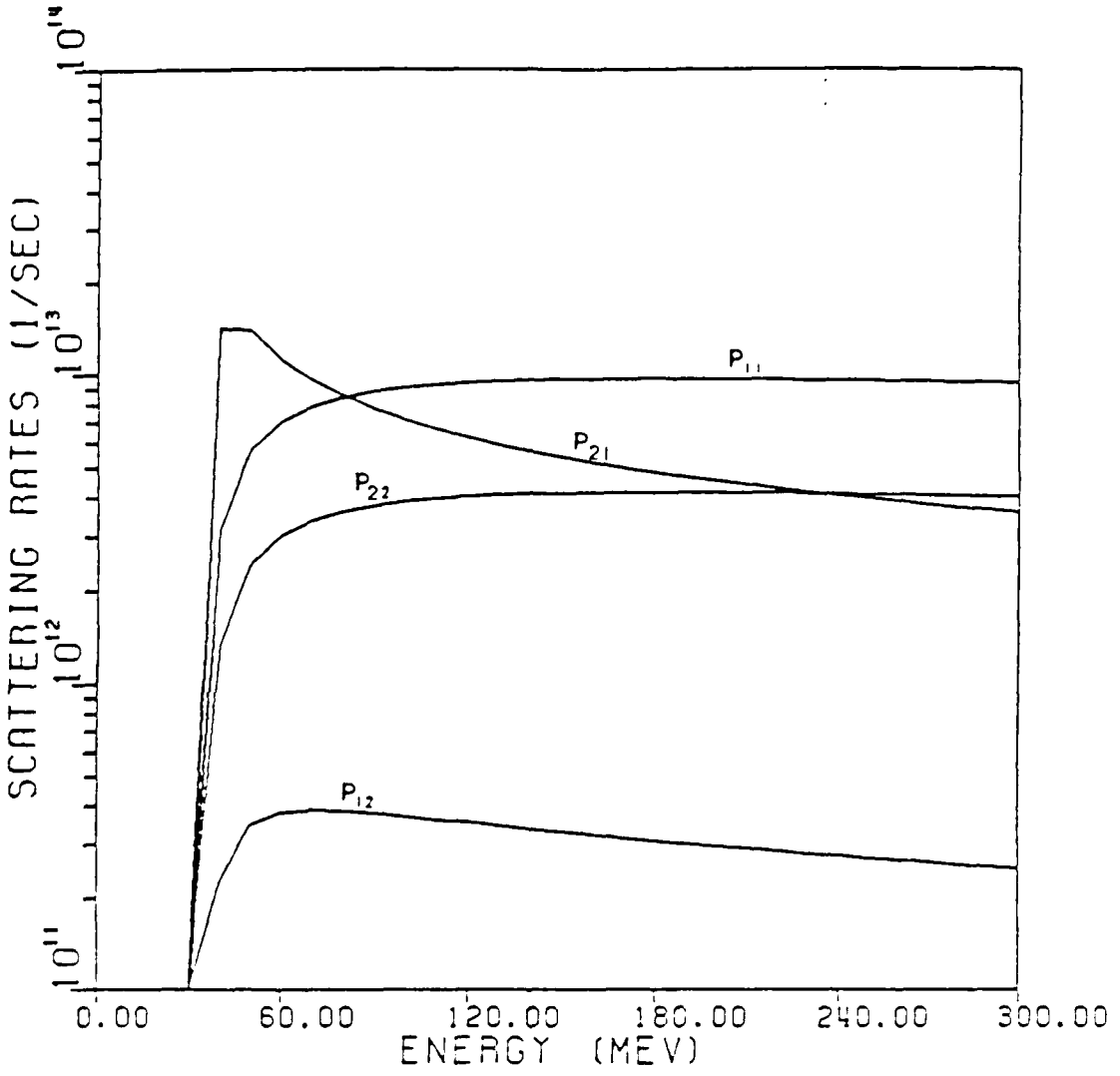

Fig. 2.8 Energy dependence of polar optical phonon emission rates for holes in GaAs at 77K.

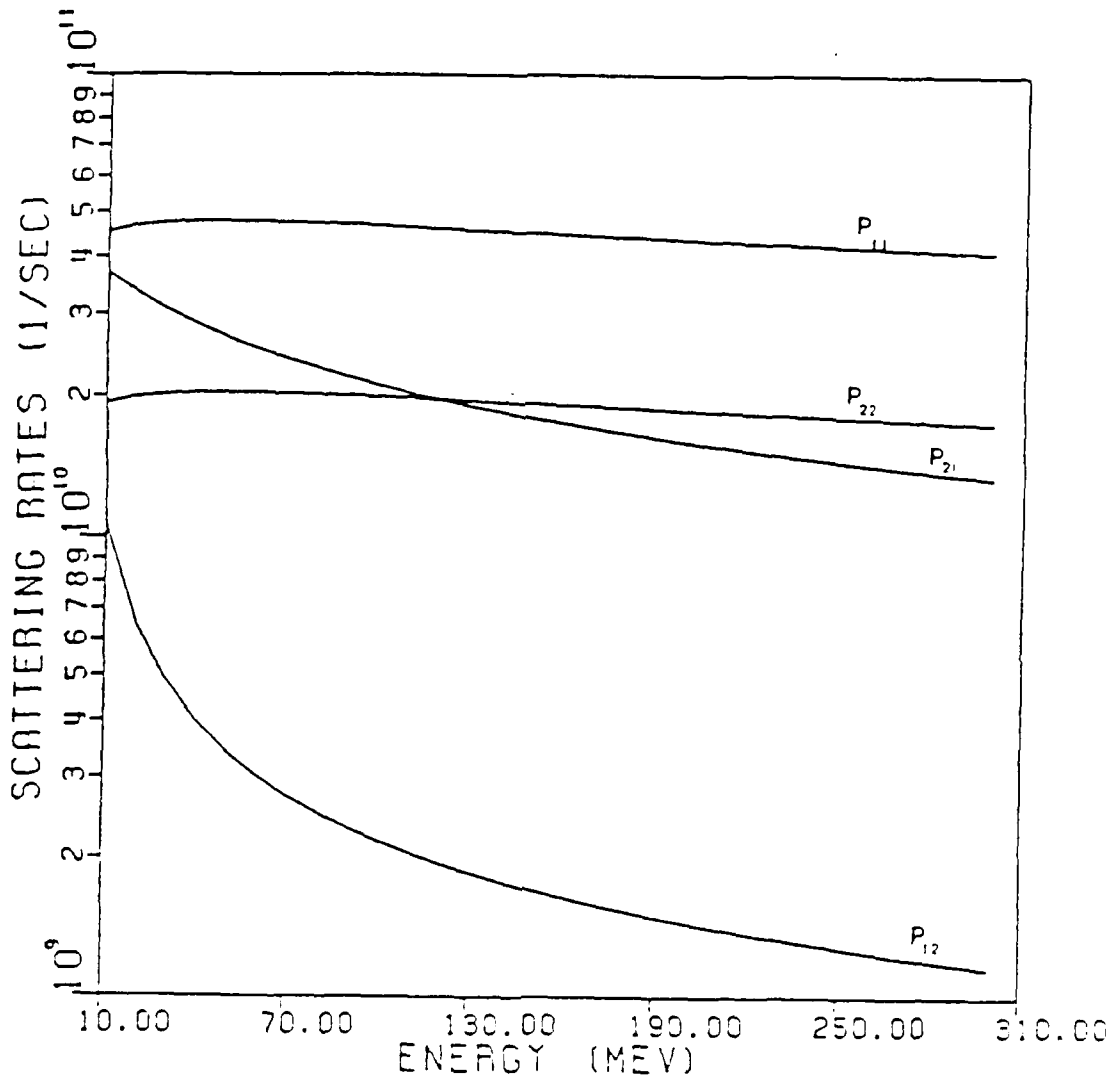

Fig. 2.9 Energy dependence of polar optical phonon absorption rates for holes in GaAs at 77K.

and n is the concentration of electrons.

2.3 Ultrafast Relaxation Mechanisms

Progress in subpicosecond laser pulse techniques has allowed direct probing of the relaxation processes of the hot photoexcited carriers in semiconductors. These works have shown that, on the picosecond time scale, a quasi-equilibrium electron-hole plasma is established through the combined action of carrier-phonon and carrier-carrier interactions. Typically, the relaxation of hot laser-excited carriers can be divided into three stages. Primarily mediated by Frohlich interactions, there is a very fast transfer of excess energy from the carriers to the LO-phonons until their mutual thermalization is reached. During this initial stage, the amount of energy received by the acoustic phonon system is negligible. In the second stage, the hot distribution cools towards the lattice temperature until optical phonons are no longer active in removing energy. The hybrid system of carriers and LO-phonons releases their excess energy to the lattice at a rate determined by the process of LO-phonons relaxing their own energy to the lattice through the anharmonic effects, while the carriers transfer their excess energy to LO-phonons to maintain a mutual quasi-equilibrium. The characteristic cooling times are much longer than those in the initial stage. The last stage involves the final cooling of the distribution to the lattice temperature through acoustic phonon emission. Sampaio and Luzzi [38] established that heating of LO-phonons, due to scattering with carriers, begins within 1 psec,

the energy transfer from carriers to LO-phonons occurs over some 5 psec, and the energy transfer from carriers to acoustic phonons occurs on a nanosecond time scale. Typically, the first two stages in the relaxation last more than 100 psec. While the subsequent cooling of this electron-hole plasma towards the lattice temperature is well studied [39], little is known about the primary stage of the carrier relaxation, and the role of electron-hole scattering. Recently, there have been several experimental investigations of the initial stage of the ultrafast relaxation done by some researchers, such as Tang and Erskine et al. [40-42,34], Oudar and coworkers [43,44] etc.

In the initial stage of the excitation process, most of the kinetic energy is given to the electron because it is much lighter than the holes. Most transitions will be from the heavy-hole band because the light holes have a much lower population. Thus, we concentrate on understanding the relaxation of the electrons in the initial stage. The electrons cascade down through the conduction band as fast as they can until their mutual thermalization. Several scattering processes will play important roles depending on the electron density. At very low densities the electrons can emit LO phonons successively and hop down the bands in units of LO phonon energy. At higher electron densities, the LO phonons and plasmons will couple together, the hopping now is in units of the coupled mode energy. At very high electron densities, the LO phonon interaction will be fully screened and the electrons will hop down the conduction band in units of the plasmon energy [43]. We should note that scattering of the

electrons by the free holes is less efficient than the electron-electron scattering in relaxing the excess energy in this stage, because most holes are much heavier than the electrons. So, in the initial stage, electron-electron scattering and polar optical phonon emission are dominant.

In the second stage of the relaxation, most carriers have interchanged most of their initial excess energy and formed a quasi-equilibrium distribution around the band edges. As discussed above, hot carriers relax basically through carrier-phonon scattering and carrier-carrier interaction. It is hard to elucidate which scattering occurs more frequently. The energy-loss-rate is a sum of three processes: LO phonon emission by both electrons and holes, and TO phonon emission by holes, because both electrons and holes can contribute to the phonon emission in the second stage [45]. The carrier-acoustic phonon interaction gives a minor contribution to the relaxation for most of the processes.

2.3.1 The Roles of Hot Phonon Effects and Screened carrier-phonon interactions in relaxation

Due solely to these carrier-phonon scattering mechanisms, the so-called "hot phonon effects" may arise, as observed experimentally [46.13]. When excess nonequilibrium LO phonons are rapidly generated in the initial stage, there results a slow carrier relaxation towards the final equilibrium with the lattice, since the nonequilibrium phonons are re-absorbed. As the generated LO phonons are larger than

the equilibrium phonon population, they follow a rapid relaxation by losing energy to zone edge modes through the anharmonic forces. One interesting result of the ultrafast relaxation experiments has been the unexpectedly slow cooling of the hot distribution. The cooling rate has generally been found to decrease with increasing carrier densities. In the case of a far-from-equilibrium electron-hole plasma, one would expect to see the consequences of production of excess phonons. The hot phonon effect emphasizes the excess phonon population, while the essential issue of the problem is phonon reabsorption by the carriers which really slows the cooling rate. The probability of phonon reabsorption increases with increasing carrier density. The lifetime of LO phonons has been measured to be approximately 7 psec in GaAs [6-8]. If the carrier density is large enough, the optical phonon will be reabsorbed before it has chances to decay. We assume that once the phonon decays, the energy is lost. Von der Linde et al. [6] showed that the anharmonic decay of the LO phonons essentially explains the lifetime in bulk GaAs.

Free carrier screening has also been confirmed to reduce the cooling rates to some extent. Nevertheless, it still is not sufficient to interpret the experimental results. However, including hot phonon effects has led to a much closer agreement [19]. Screening will affect which modes become hot, and the degree to which the phonon population is disturbed. Furthermore, screening is very effective at reducing the scattering of electrons by the Frohlich interaction since this interaction is strongest at small q-vectors, where screening is most significant. Screening has less influence on holes than

electrons because of the large q-vectors related to holes. It has been recognized that the cooling process, during the first few picoseconds, is mainly influenced by the carrier-carrier interaction, the hot phonon effects, the screened LO-phonon interaction, and the optical deformation potential interaction for holes. A refined analytical model to determine the relative importance of the roles played by electron-hole interaction, phonon heating, and free-carrier screening on the reduction of the cooling rates has been proposed recently by Pötz [19].

2.3.2 The Role of Electron-Hole Interaction in Relaxation

Carrier-carrier scattering manifests a different behavior at different carrier densities. It affects the relaxation process basically in two aspects. First, it gives rise to screening, which changes the strength of other scatterings. Second, it tends to redistribute the energy among the carriers for reaching a quasi-equilibrium distribution which may be described simply by an effective temperature. However, the latter statement is found to be true only on time scales greater than one or two picoseconds, where the carriers have really already thermalized among themselves and their distributions may be approximated by parameterized Maxwell-Boltzmann or Fermi-Dirac distributions [36]. Since one of the purposes of this thesis is to examine the role of the electron-hole interaction on the cooling process, we emphasize the electron-hole interaction rather than the other carrier-carrier interactions.

Since the initial energy of the electrons is much higher than the holes, the electron-hole plasma forms a far-from-equilibrium system. One would expect the energy to be transferred from the hot electrons to the cold holes and to the lattice, through the electron-hole interaction and carrier-phonon interaction, respectively. At low excitation levels the energy flow is dominated by the electron-phonon interaction, while at high excitation levels the energy is mainly channelled via electron-hole interaction to the holes and then via the TO phonon emission by the holes, due to the unscreened deformation potential interaction with the lattice. This is understandable, because at high carrier densities the electron-phonon interaction is highly screened while the electron-hole interaction becomes stronger. Since the electron-hole scattering rate is high, a large fraction of each electron's energy will eventually be channelled to the holes when an equilibrium is reached between the electron and hole systems. In addition, the electron-hole interaction slows the cooling rates at low carrier densities by gradually shifting the electron population to the lower energy states. However, it enhances the cooling rate at high carrier densities because the electrons can transfer energy to the lattice through the holes. Fig. 2.10 fully depicts the energy flowing channels for laser-excited system at different carrier densities. A first experiment investigating the electron-hole energy transfer in semiconductors has been reported by Höpfel and coworkers [14] recently. They observed that the energy-loss-rate of hot minority electrons in a cold hole plasma is higher by about a factor of two than that of majority electrons in the absence of holes.

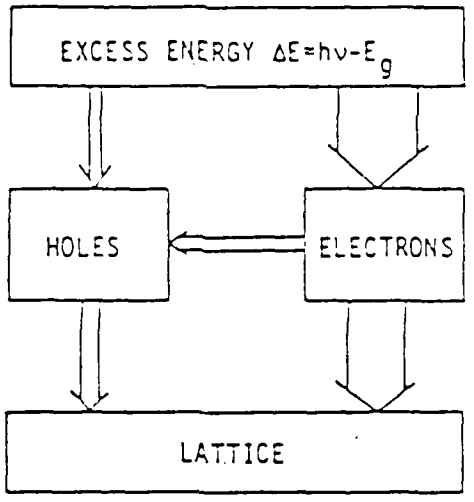

a

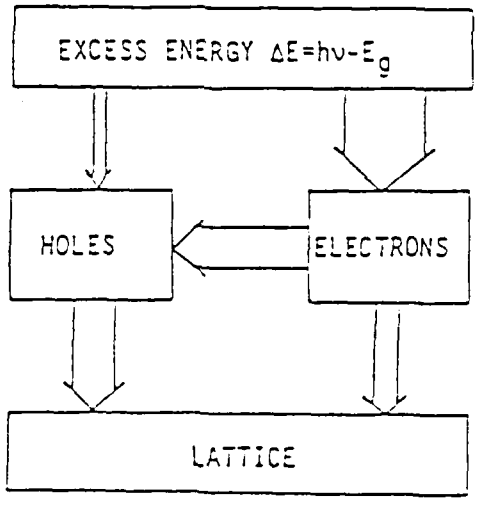

b

Fig. 2.10 Energy flow channels from the pulse to the lattice in GaAs at 77K, $h\nu=1.64$; a) $n=5\times10^{16}cm^{-3}$, b) $n=1\times10^{18}cm^{-3}$.

CHAPTER 3

ENSEMBLE MONTE CARLO TECHNIQUES FOR HOT PHOTOEXCITED CARRIER RELAXATION

3.1 Boltzmann Transport Theory

As a preliminary to any statistical discussion of nonequilibrium processes, one must find a way to evaluate the distribution function when the system is nonequilibrium. This is accomplished by means of the Boltzmann equation. If the rate of change of the distribution function due to collisions or scatterings is denoted by $\left(\frac{\partial f}{\partial t}\right)_{coll}$, then the total rate of change of the distribution function f can be expressed as

$$\frac{df}{dt} = -\vec{v}\cdot\frac{\partial f}{\partial \vec{r}} - \frac{e\vec{F}}{\hbar}\cdot\frac{\partial f}{\partial \vec{k}} + \left(\frac{\partial f}{\partial t}\right)_{coll}, \tag{3.1}$$

where $\vec{F}$ is the applied external field and $m\vec{v} = \hbar\vec{k}$ is the momentum. The first and second term on the right hand side of (3.1) represent the effect of the density gradient and of the applied external field on the distribution function. In semiconductors, the behavior of carriers is affected by the applied external field, density gradient, and scattering from phonons, impurities or other carriers etc. All these factors can be included in the Boltzmann transport equation to obtain information about the carrier distribution function f. This semi-classical integro-differential equation for f can be solved

numerically with the help of fast computers. Otherwise, some simplifying assumptions have to be made in order to solve the equation analytically under certain special conditions. The most generally used analytical methods are the Legendre polynomials expansion and the displaced Maxwellian approximation [47]. One of the numerical techniques is the iterative method, while the other one is the Monte Carlo method on which we focus our attention.

3.2 Application of Ensemble Monte Carlo Method to Transport in Semiconductors

The Monte Carlo method was first applied to the transport in semiconductors by Kurosawa (1966) to study steady-state hole transport in Ge. It is a very powerful numerical technique, because it can simulate special physical situations which are unachievable in experiments, and also investigate the non-existing materials to examine important features of phenomenon in which we are interested. Since this stochastic evaluation of the solution of the Boltzmann transport equation is a direct way to simulate the dynamics of the carriers inside semiconductors, any physical information can be easily obtained while the time-evolving solution of the equation is being determined. The single particle Monte Carlo method is extended to a many-particle ensemble Monte Carlo method in order to investigate non-steady-state or non-homogeneous phenomena in semiconductors. A general flow chart of the ensemble Monte Carlo program is given in Fig. 3.1.

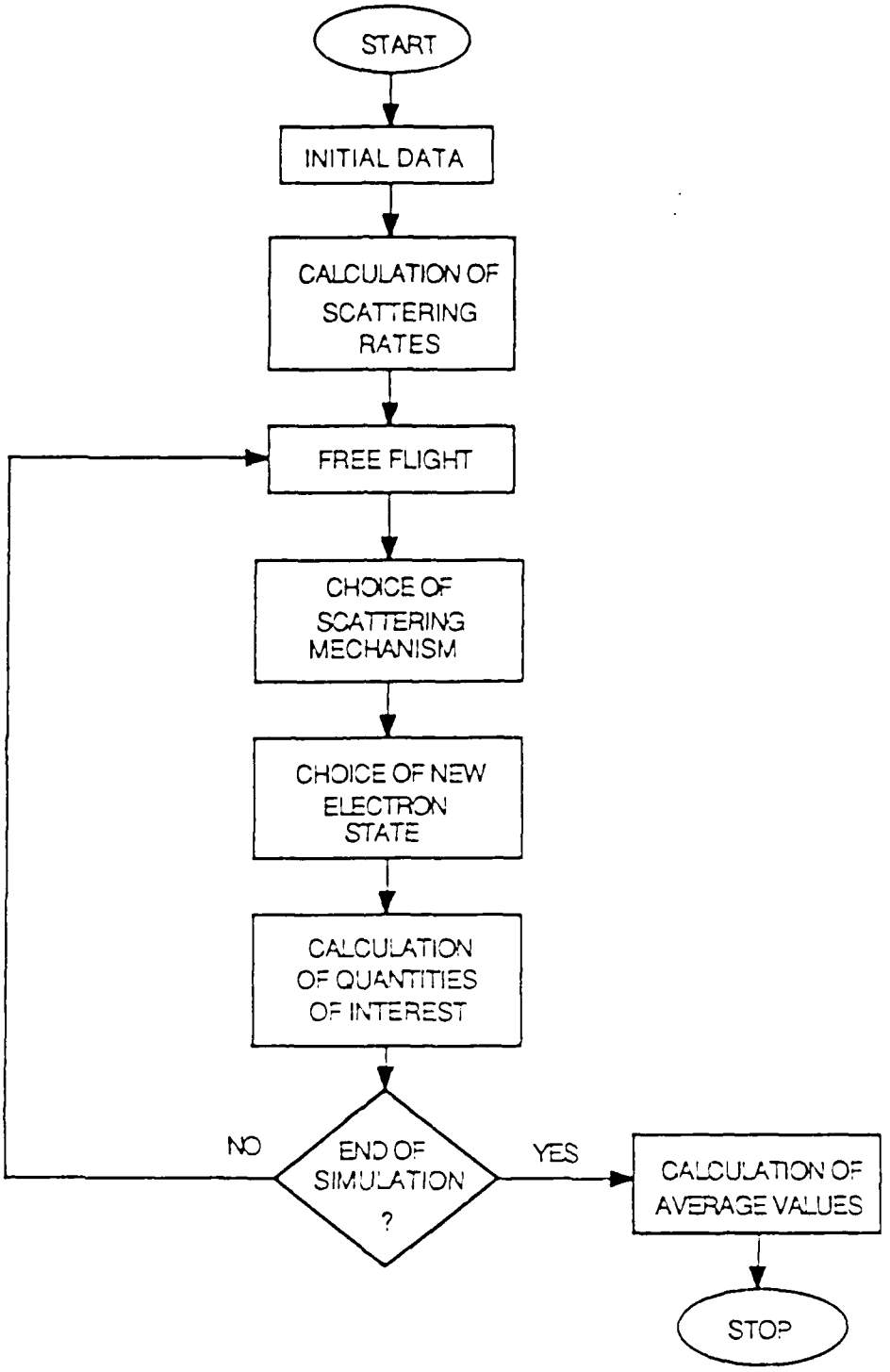

Fig. 3.1 Flow chart of a Monte Carlo program.

The semiclassical EMC method contains simulations of the motion of an ensemble of charge carriers inside the semiconductor with (or without) an electric field applied and with the scattering mechanisms specified. The scattering probabilities of each scattering mechanism are calculated and tabulated inside subroutines of the program. The alternative sequence of drifts and instantaneous collisions with phonons, impurities or other carriers are iteratively simulated, relying on the generation of a sequence of random numbers. A special method to determine the free flight time without solving a complicated integral equation directly was devised by Rees [54], who introduced a fictitious "self-scattering" so that the total scattering probability, including this self scattering, is equal to a constant Γ which is taken to be at least as large as the largest value of the total scattering rates. Then, $P_0(E) = \Gamma - P(E)$ is the probability of self scattering. If a carrier undergoes such a self scattering which is of no physical significance and does not change the distribution function, its final $\vec{s}$tate after collision is the same as the initial state before the scattering, so that the electron motion remains unperturbed as if no scattering occurred at all. A random number r distributed between 0 and 1 can be used to generate a stochastic free flight time t_r, where

$$t_r = -\frac{1}{\Gamma}\ln r.$$

It is advantageous to make Γ as small as possible in order to minimize the number of self-scattering events [9]. The computer time wasted in

taking care of self-scattering is more than compensated by the simplification of the calculation required to determine the free flight time. Having determined the free flight time, it is necessary to determine which scattering process terminates the free flight. The arbitrary choice of the scattering mechanism for a particular carrier with energy E is also determined by the random numbers. Since the probability of the electron being scattered by process i is proportional to the scattering rate $P_i(E)$ for the ith mechanism, and since $\sum_{i=0}^{N} P_i(E) = \Gamma$, it is necessary to generate a random number r between 0 and 1 to test the inequality $r\Gamma < \sum_{i=1}^{m} P_i(E)$ for all m. When this inequality is satisfied the mth scattering process is chosen. Figure 3.2 illustrates how a mechanism is picked, as elucidated. If all scattering processes have been tried and none has been selected, it means that $r\Gamma > P(E)$, and a self scattering occurs, where $P(E) = \sum_{i=1}^{N} P_i(E)$. The energy of the final state is determined by the properties of the chosen scattering process, while the determination of the orientation of the final wave-vector requires further generation of random numbers to determine the angles θ and ϕ (see Fig. 3.3) according to the angular dependence of the chosen scattering process described in Chapter 2.

This EMC method traces the history of an ensemble of carriers, in parallel, for successive very short time intervals, instead of following the path of a single particle for a long period of time. Each carrier in the ensemble can be described by a set of physical variables $\{Q_i\}$ that fully describe the carrier's state. Since every

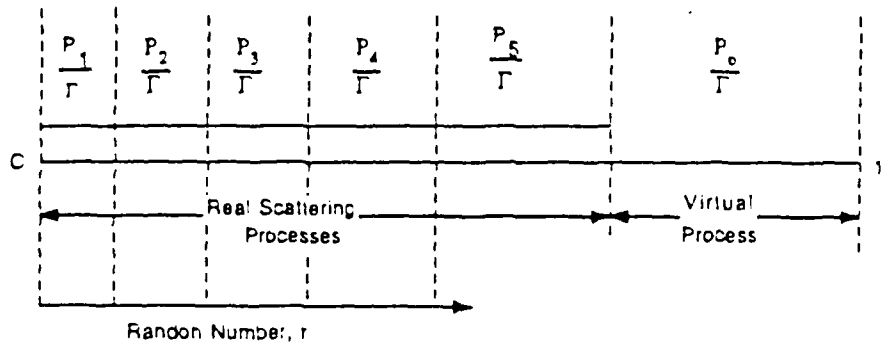

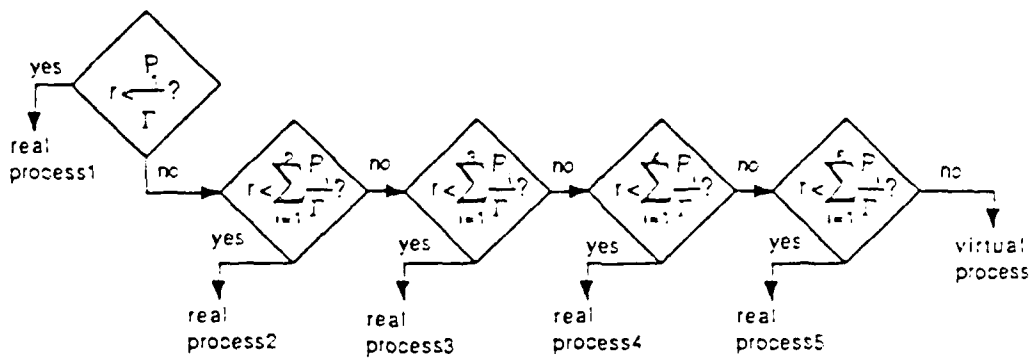

Fig. 3.2 Selection of scattering process in Monte Carlo method.

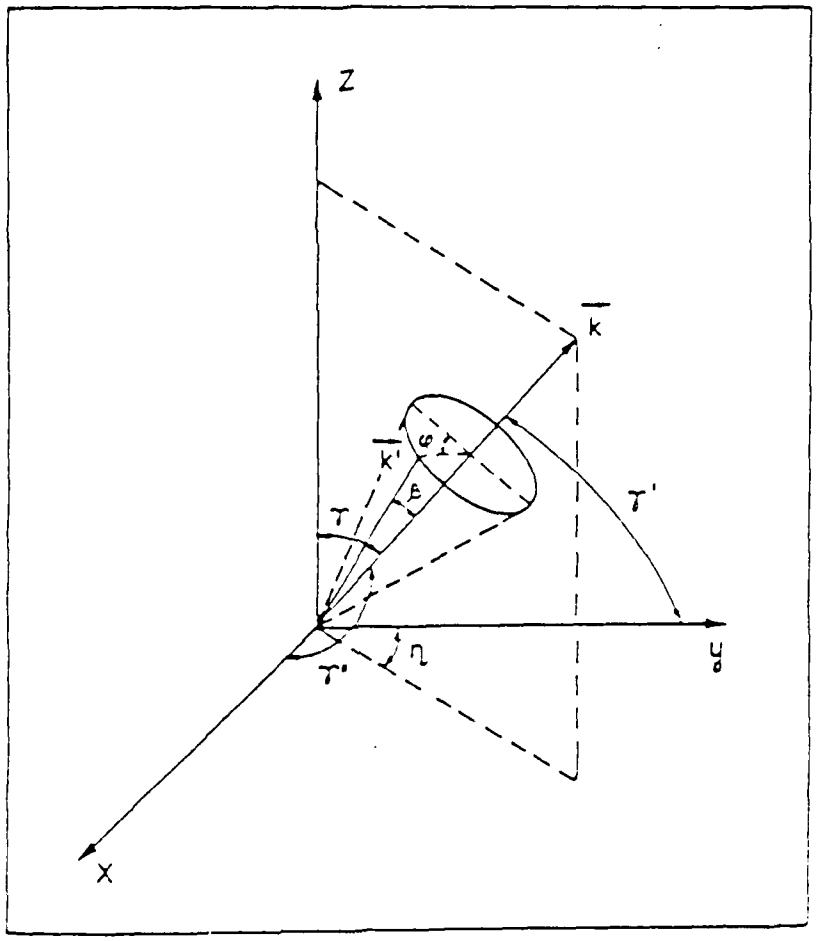

Fig. 3.3 Geometry for the determination of the state after scattering when full three-dimensional simulation is performed

Q_i is calculated at each time step using the MC method, the set $\{Q_i\}$ is also an ensemble evolving in time. The average value of a quantity Q is defined as the ensemble average at time t over the N carriers of the system,

$$\langle Q \rangle = \frac{1}{N_i}\Sigma Q_i(t).$$

3.3 Ensemble Monte Carlo Model for Electron-Hole Interaction

It is very hard to evaluate the carrier-carrier scattering rates analytically because one has to assume the shapes of the distribution functions f_e, f_h involved in the integrals as expressed in (2.4) and (2.5). However, one of the beauties of the EMC technique is that, there is no need to manipulate the complex integrals analytically since the scattering rates can be expressed as the ensemble averages in the following,

$$P_{eh}(\vec{K}_1) = \frac{pue^4}{2\pi\varepsilon^2\hbar^3}\frac{1}{N_h}\Sigma_i \frac{Q_{eh}}{\beta^2\left(Q_{eh}^2+\beta^2\right)},$$

$$P_{he}(\vec{K}_1) = \frac{nue^4}{2\pi\varepsilon^2\hbar^3}\frac{1}{N_e}\Sigma_i \frac{Q_{he}}{\beta^2\left(Q_{he}^2+\beta^2\right)},$$

where N_h, N_e are the total numbers of electrons and holes in the ensemble respectively.

3.3.1 Description of Flow Chart of the Model

A flow chart of the EMC program developed to study the relaxation of the hot photoexcited carriers is illustrated in Fig. 3.4. The initialization step gives the material parameters, the initial distribution of carriers, and other input parameters needed to investigate the relaxation such as the number of iterations, the observing time, lattice temperature, the photon energy and pulse duration, the flags to specify particular conditions of interest, etc. The second step is to calculate and tabulate the scattering probabilities for each mechanism, such as acoustic, polar optical, non-polar optical scatterings, etc. which are all calculated without screening in this step. The third step is photoexcitation. During this step, the electron-hole pairs are generated according to the given pulse shape and the energies are distributed to the carriers according the band structure. Also, the spatial distributions of the photo-generated carriers are determined. The fourth block is to calculate the carrier-carrier scattering rate using the formulae developed above. Simultaneously, the self-consistent screening length is also determined for calculating the screened carrier-phonon scattering rates. The fifth block is to calculate the screened carrier-phonon scattering rates using the screening length calculated previously. The dynamics of [illegible] investigated using EMC method seperately. [illegible] EMC, because, once the [illegible] must be selected from the [illegible] EMC is

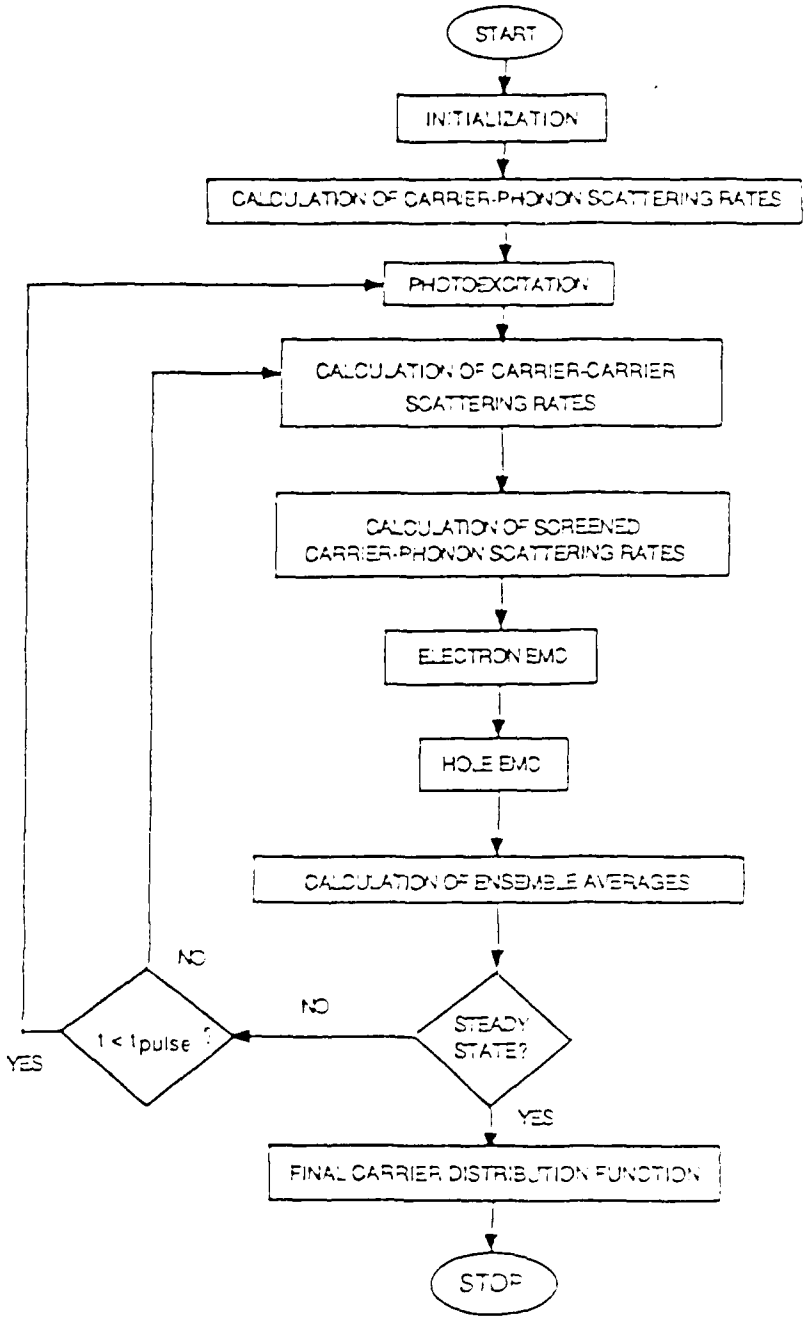

Fig. 3.4 Flow chart of the ensemble Monte Carlo Program for electron-hole interaction.

coupled to the electron EMC because of the hole-electron scattering. It is noted that the scattering rates of electron-hole scattering and hole-electron scattering are different. In the eighth block, the ensemble averages of interest are calculated, such as the mean energy of carriers, the equivalent carrier temperature, or drift velocity etc. Additionally, the energy and momentum distributions of carriers are specified in this block too. When the pulse is still on, steps 3~8 are repeated. Only steps 4~8 are repeated when the pulse is over.

3.3.2 Self-Consistent Screening Model

Apparently, the screening length has great influence on the screened carrier-phonon and carrier-carrier scattering rates. Several analytical models for calculating the screening length have been reported showing that the magnitude of the screening length varies with different models. A self-consistent screening length in the static and long wavelength limit of the random phase approximation calculated in the EMC method, taking advantage of its built-in time-evolving distribution functions, has been developed recently [55]. The way it is calculated is described in the following. The dielectric constant $\varepsilon(q,\omega)$ is given by

$$\varepsilon(q,\omega) = 1 - \frac{e^2}{\varepsilon_\infty q^2} \sum_k \frac{f(k)-f(k+q)}{E(k+q)-E(k)-\hbar\omega}. \qquad (3.2)$$

In the static and long wavelength case, (3.2) becomes [56]

$$\varepsilon(q,0) = 1 + \frac{e^2}{\varepsilon_\infty q^2}\int\left(-\frac{\partial f(E)}{\partial E}\right)D(E)dE$$

$$= 1 + \frac{\beta^2}{q^2},$$

where D(E) is the density of states and β is the inverse of screening length given as

$$\beta^2 = \frac{e^2}{\varepsilon_\infty}\int\left(-\frac{\partial f(E)}{\partial E}\right)D(E)dE \tag{3.3}$$

$$= \frac{e^2}{\varepsilon_\infty}\int\left(\frac{\partial D(E)}{\partial E}\right)f(E)dE. \tag{3.4}$$

For convenience, we define B(E) as

$$\frac{\partial D(E)}{\partial E} = B(E)D(E). \tag{3.5}$$

Obviously, B(E) is the logarithmic derivative of the density of states D(E). Inserting (3.5) into (3.4), we obtain

$$\beta^2 = \frac{e^2}{\varepsilon_\infty}\int B(E)D(E)f(E)dE,$$

$$= \frac{ne^2}{\varepsilon_\infty}\langle B(E)\rangle \tag{3.6}$$

where

$$\langle B(E) \rangle = \frac{\int B(E)D(E)f(E)dE}{\int D(E)f(E)dE},$$

and the carrier concentration n is defined as

$$n = \int D(E)f(E)dE.$$

From (3.6), we see an amazing result showing that β^2 can be expressed in terms of the ensemble average of B(E) and is given as

$$\beta^2 = \frac{ne^2}{\varepsilon_\infty} \frac{1}{N} \sum_i B(E_i), \tag{3.7}$$

where N is the number of carriers in the ensemble. The form of B(E) depends on the band model used in the EMC calculation. For parabolic bands, B(E) is given as

$$B(E) = \frac{1}{2E}.$$

For nonparabolic bands, B(E) becomes

$$B(E) = \frac{2\alpha}{1+2\alpha E} + \frac{1+2\alpha E}{2E(1+\alpha E)}.$$

While assuming a Maxwell-Boltzmann distribution function, (3.6) becomes

$$\beta^2 = \frac{ne^2}{\varepsilon_\infty k_B}\left[\frac{1}{T_e} + \frac{1}{T_h}\right],$$

which is the screening length of the Debye-HÜckel screening model. T_e and T_h are the electron and hole temperatures, respectively. The cooling rate predicted by the Debye-HÜckel model is slower than the one calculated by the self-consistent screening model, which means the Debye-HÜckel model overestimates the screening. The results of the comparisons will be discussed in the next chapter.

3.4 Ensemble Monte Carlo Model for Hot Phonon Effects

In addition to the difficulties needed to be overcome in programming, the electron-electron and hole-hole interactions, and the screening of carrier-phonon interactions, as well as electron-plasmon scatterings are all ignored in this simulation to better demonstrate the hot phonon effects and electron-hole interactions. The time-evolving LO-phonon distribution function is specified and the modified scattering rates of the electrons due to the nonequilibrium phonon population are recalculated. We only consider the disturbance of the LO-phonons while ignoring the other types, because the LO-phonons play a major role in most of the cooling process. The algorithm developed to study the hot phonon effects, which slows down the electron relaxation in the bulk laser-excited GaAs, will be discussed below.

First, we need to set up a histogram h_q defined over the $\vec{q}$ space for the LO-phonons in the program to follow the time-evolving phonon distribution. After each time step, in which the electron suffers a collision involving an LO-phonon, the histogram is updated. At fixed successive time intervals ($n\Delta t$), where Δt is always much shorter than

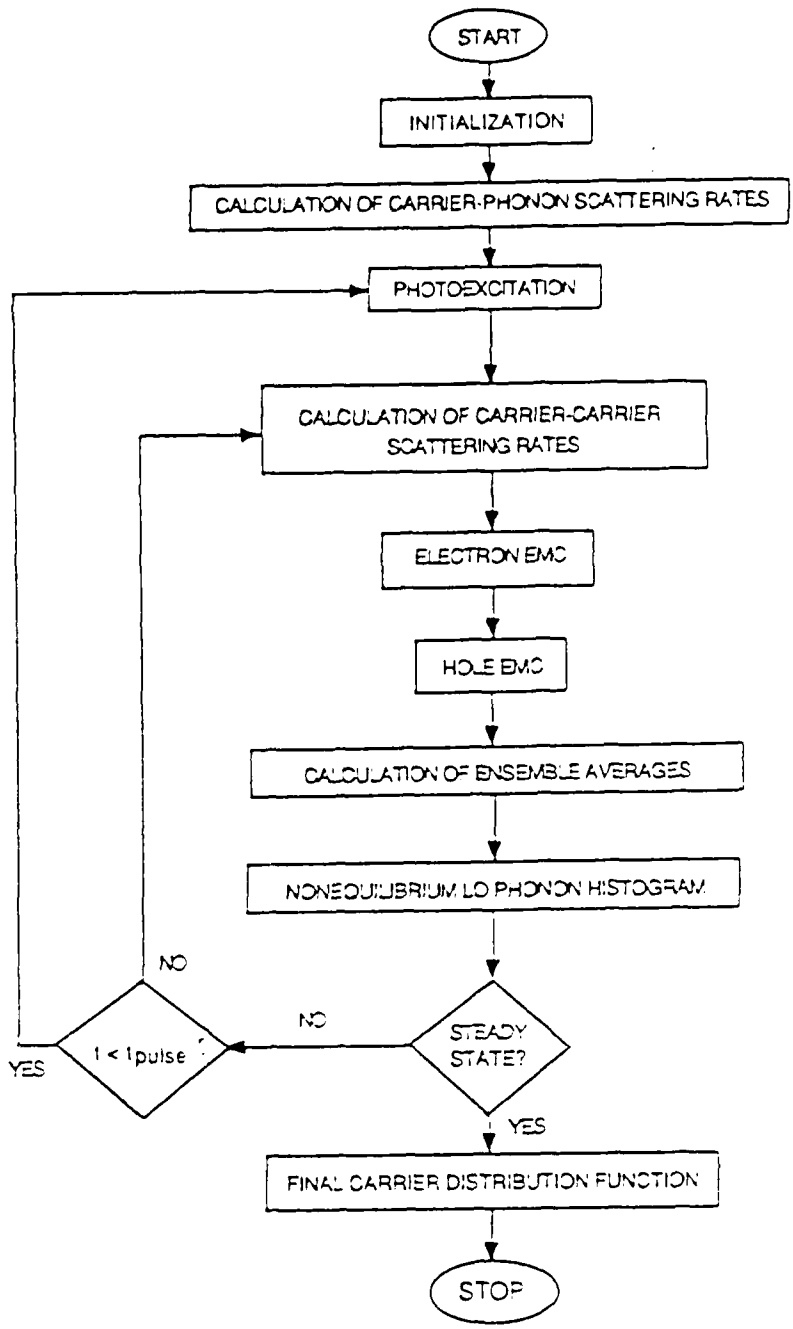

Fig. 3.5 Flow chart of the ensemble Monte Carlo Program for hot phonon effects.

the average scattering time for the LO-phonon scattering, N_q can be calculated by [25]

$$N_q(n\Delta t) = \bar{N}_q(n\Delta t) - \left[\bar{N}_q(n\Delta t) - N_o\right]\frac{\Delta t}{\tau}, \qquad (3.8)$$

where

$$\bar{N}_q(n\Delta t) = N_q[(n-1)\Delta t] + A\Delta h_q,$$

and N_o is the equilibrium Bose-Einstein phonon distribution function. The term $A\Delta h_q$ gives the dynamical contribution of the electronic processes to the phonon distribution during the time step Δt, where A is a normalization factor accounting for the density of states in $\vec{q}$ space and for the concentration of excited electrons. A is given as

$$A = \frac{n2\pi^2}{Nq^2(\Delta q)},$$

where n is the concentration of electrons in the central valley, N is the total number of electrons in the ensemble, q is the phonon wave vector, and Δq is the incremental grid element of phonon wave vector in the histogram. The second term on the right hand side of (3.8) represents the phonon-phonon processes with an experimentally determined LO-phonon relaxation time τ of 7 ps [6]. In Lugli's paper [25], the scattering rates concerning the LO-phonons are recalculated at every fixed time interval ($n\Delta t$) according to the new time-evolving phonon distribution function given by (3.8), so that, the

modifications resulting from the phonon disturbance are taken into account. Here, instead of recalculating the scattering rates for the LO-phonons using the perturbed phonon distribution, a very large number chosen at the beginning of the simulation has been used for the maximized nonequilibrium phonon distribution function to calculate the scattering rates for LO-phonons and then a rejection method is used to determine the final state after each scattering process involving an LO phonon [57]. The algorithm expressed above has been used to study the relaxation process of the bulk GaAs at nitrogen temperature (77 $^{\circ}$K) illuminated by a laser pulse of either delta pulse shape or 0.2 ps pulse duration. The results of the calculations will be discussed in next chapter.

CHAPTER 4

RESULTS AND DISCUSSIONS

The influences of the electron-hole interaction and hot phonon effects to the ultrafast relaxation of hot laser-excited carriers in GaAs were investigated via the ensemble Monte Carlo method for different excitation levels, ranging from $5x10^{16}$ to $1x10^{18}$ cm^{-3}, at different excitation energies. The pulse duration was taken to be a delta function for convenience in the calculations. Additionally, the cooling rates of the photoexcited carriers, while disregarding carrier-carrier interactions, were evaluated using both the Debye-HÜckel and the self-consistent screening models which have already been built in the program. The results of the simulations will be discussed and compared in the following sections.

4.1 The Effect of Electron-Hole Interaction

The initial mean energy of the excited electrons is about seven times the corresponding energy of holes, according to the band structure of GaAs, so that the electron-hole plasma forms a far-from equilibrium system. Accordingly, the energy is transferred from the hot electrons to the cold holes and then to the lattice through the electron-hole and carrier-phonon scatterings. In this section, the manner in which the electron-hole interaction affects the role of the electron-phonon interaction, which dominates the cooling processes,

was examined. The phonons were assumed to be in thermal equilibrium in this situation.

The time evolution of the electron mean energy is shown in Fig. 4.1 to illustrate how the electron-hole interaction behaves under different carrier concentrations. It is found that the cooling rate slows down as the excitation level increases under the situation where only unscreened carrier-phonon and electron-hole interactions were active. The holes are expected to behave the same way. The relative importance of the electron-phonon and electron-hole interactions as energy transfer channels depends on the excitation level and excitation energy. From Fig.4.2, it is found that the electron-hole interaction promotes the cooling rate at high excitation levels because the hot electrons transfer their excess energy to the lattice through the holes mainly by emission of TO phonons via the unscreened optical deformation potential coupling. However, the electron-hole interaction slows down the cooling rate at low excitation level as shown in Fig. 4.3 because the electron population was shifted gradually to lower energy states via the electron-hole scatterings[58].

It is obvious that the electrons cool faster at lower excitation levels as shown in Fig. 4.1 where the screening is negligible. The slowing becomes more significant at high carrier densities, where the optical phonons are strongly screened and the electron-electron scatterings occur more frequently. The electron-electron and hole-hole interactions were ignored in this calculation because of the complications of some major changes in the program. However, it is

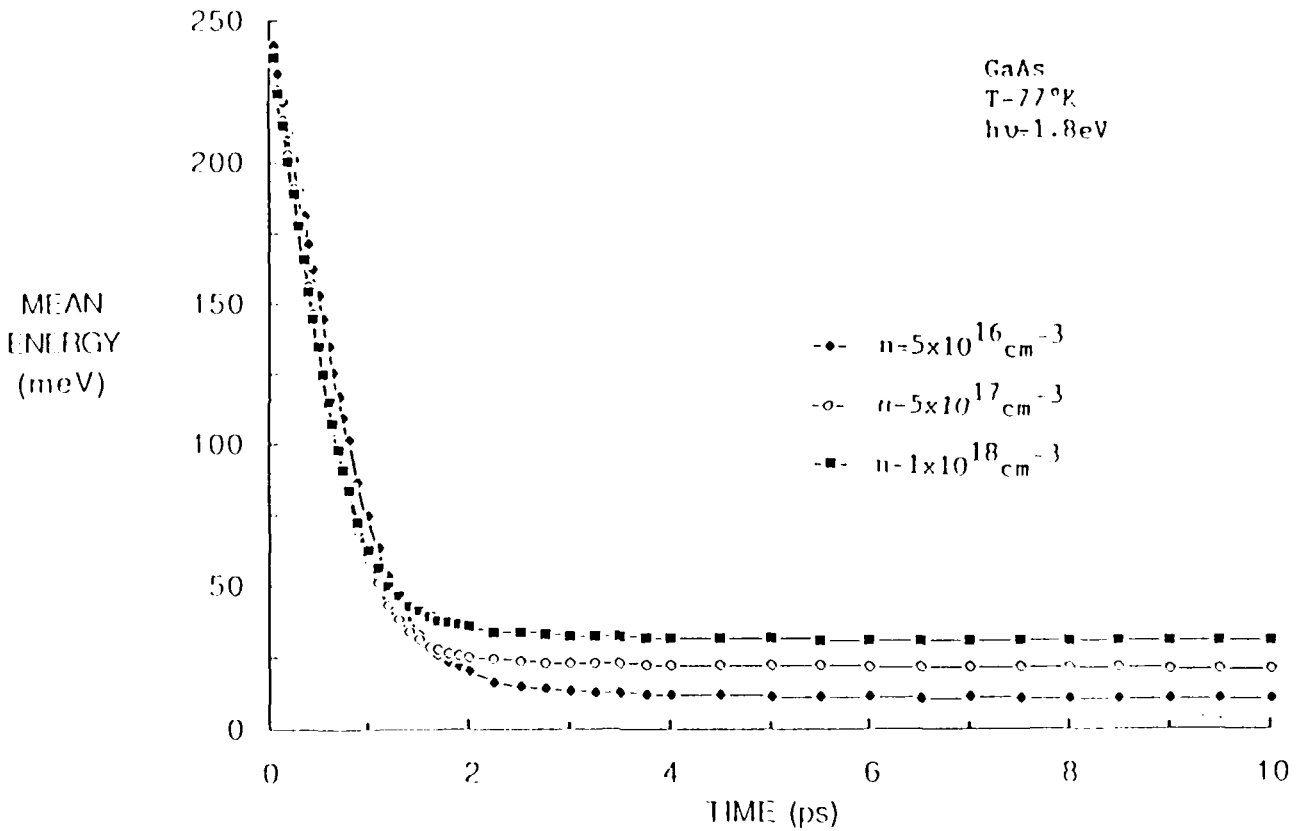

Fig. 4.1 The time evolution of electron mean energies with different excitation levels.

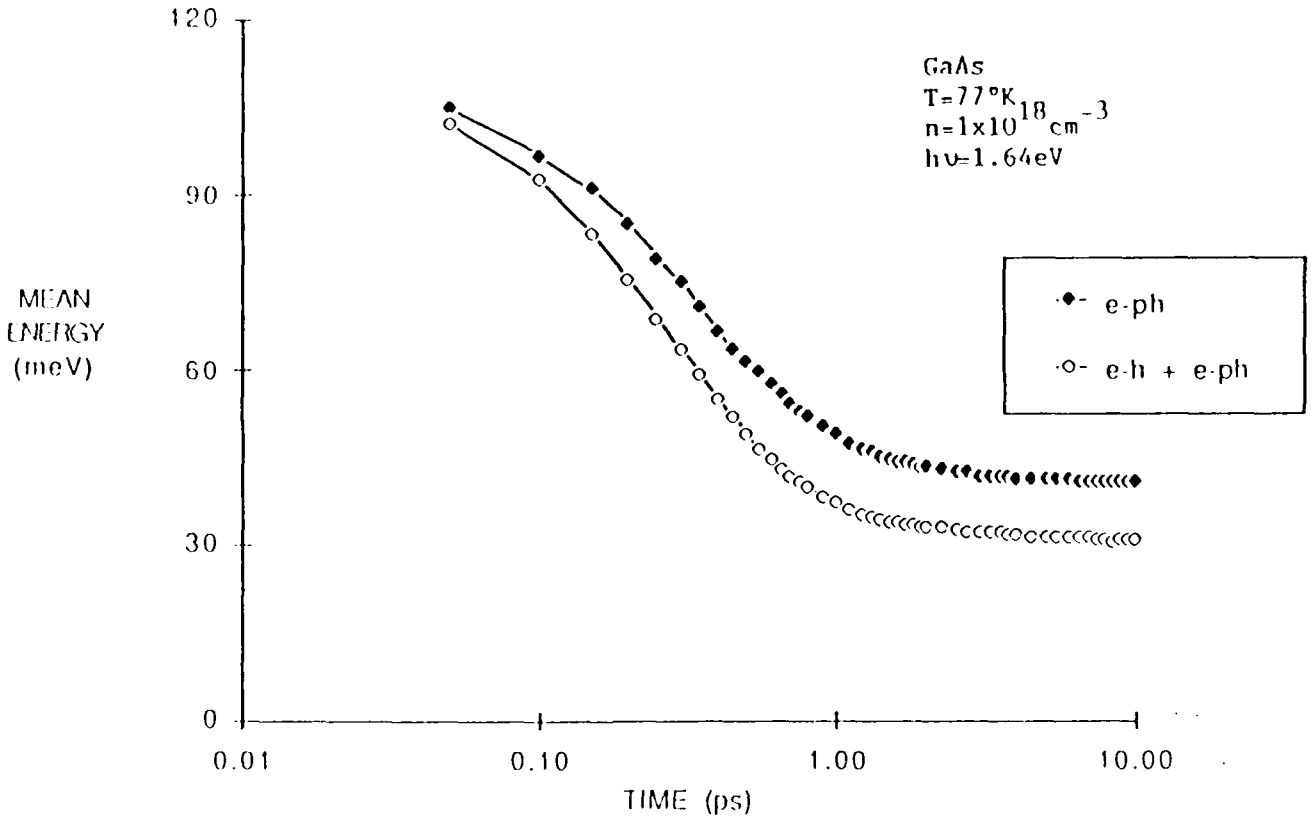

Fig. 4.2 The time evolution of electron mean energy for various scattering mechanisms. The electron-hole interaction enhances the cooling rate of electrons.

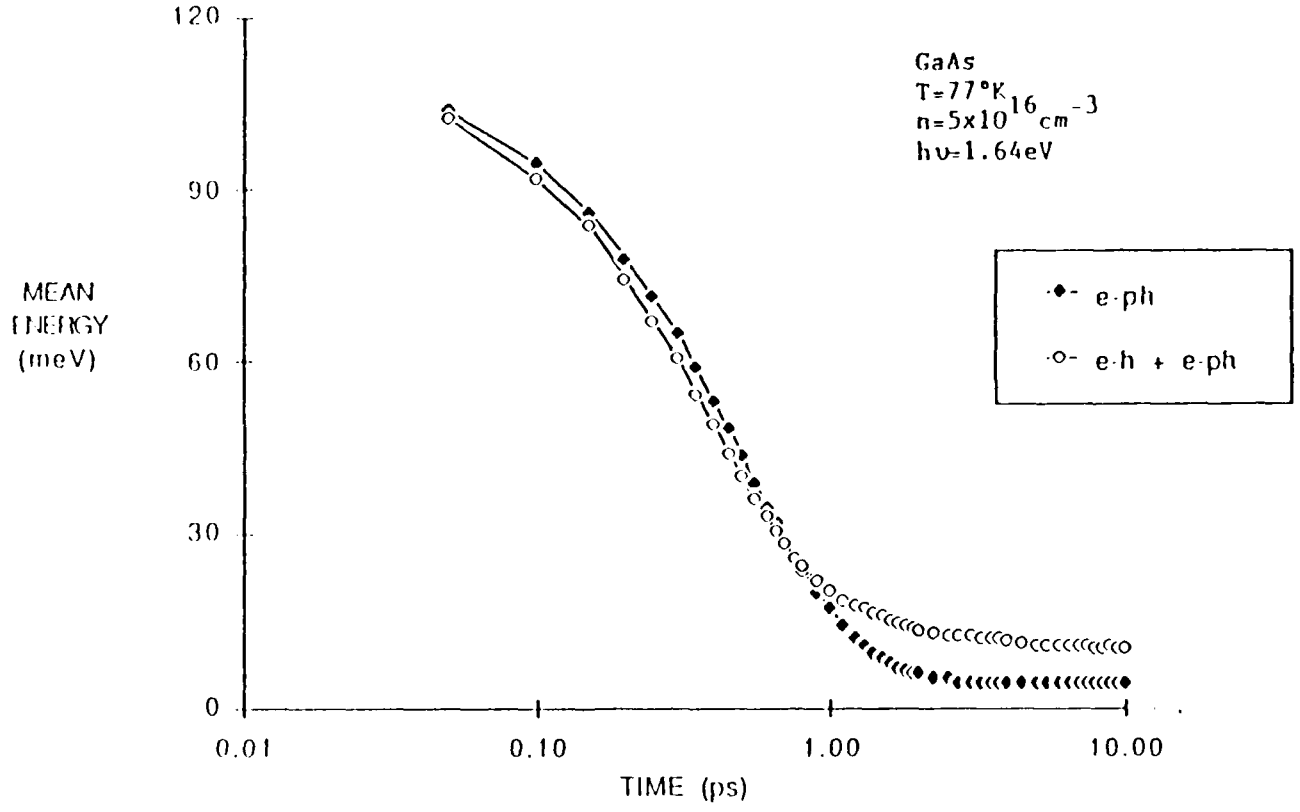

Fig. 4.3 The time evolution of electron mean energy for various scattering mechanisms. The electron-hole interaction slows down the cooling rate of electrons.

anticipated that the hole-hole scatterings enhance the cooling of the hole system while the electron-electron scatterings slow the cooling of the electrons. The reason why the cooling of the holes is enhanced can be resorted to the fact that the hole-hole scattering rate is very high so that the hole-hole scatterings kick some holes above the phonon emission threshold, and these then emit phonons through the deformation potential interaction. On the other hand, the interaction among the electrons quickly redistributes the electrons into high and low energy regions[36].

4.2 The Role of Hot Phonon Effects

The model used to examine the hot phonon effects is basically based on the model proposed by Lugli and coworkers[25]. This model takes account of the electron-hole and non-equilibrium LO phonon-electron interactions. Electron-electron, hole-hole, and electron-plasmon interactions and the screening of carrier-phonon interactions were ignored here. The effect of hot phonons was examined for an excitation energy of 1.8 ev, which does not exceed the band gap of 1.51 eV too much, in order to prevent complications caused by exciting electrons to the upper valleys. It is found that the non-equilibrium phonons do slow down the cooling rate of the hot laser-excited electrons further, as shown in Fig. 4.4, by comparing with the results obtained from the situation where only the unscreened carrier-phonon and the electron-hole interactions were active. This phenomenon is mainly caused by the reabsorption of previously emitted LO phonons

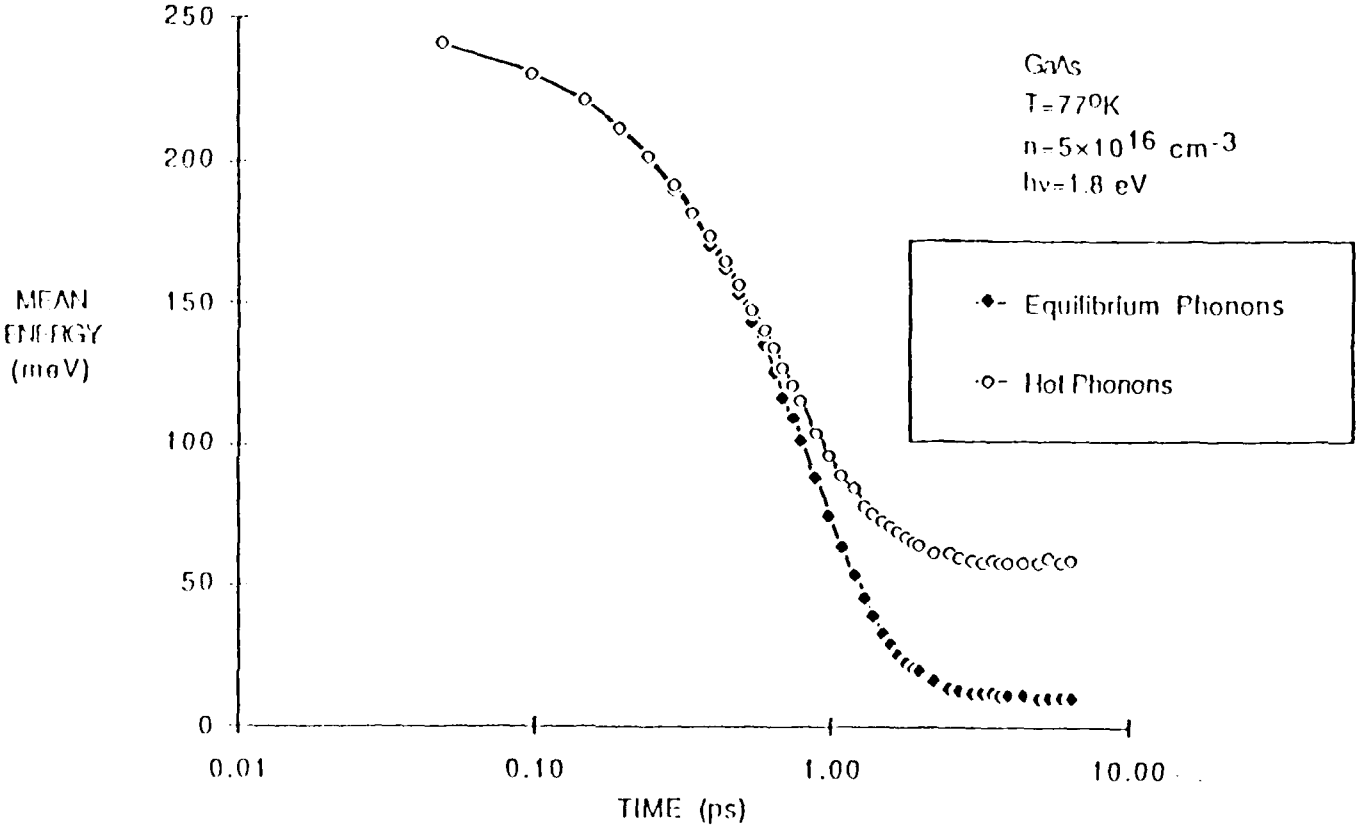

Fig. 4.4 The effect of the non-equilibrium LO phonons is to further slow the decay of the energy.

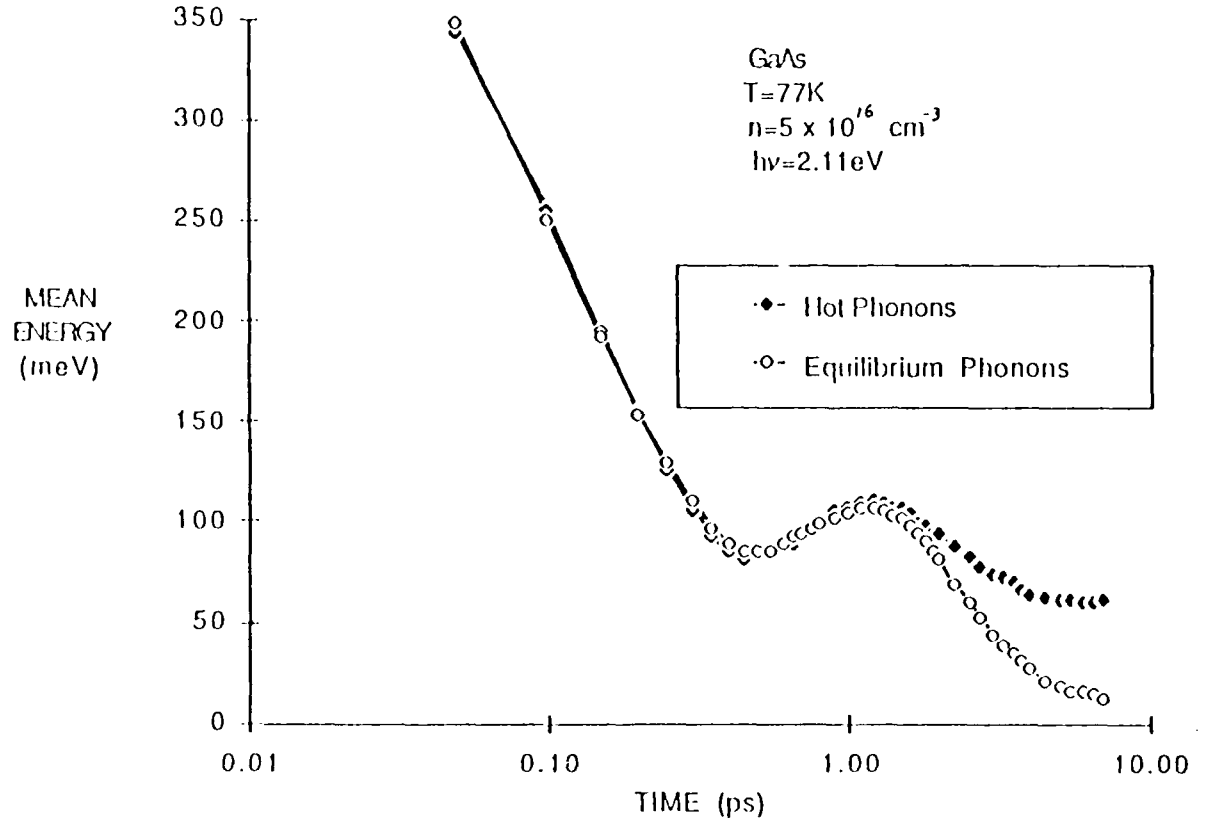
GaAs
T=77K
n=5 x 10^16 cm^-3
hν=2.11eV
Hot Phonons
Equilibrium Phonons
MEAN ENERGY (meV)
350
300
250
200
150
100
50
0
0.01
0.10
1.00
10.00
TIME (ps)

without having enough time to decay into near-zone boundary phonons, which would not couple back to the electrons, as well as the thermalization of the electrons and holes. In Fig. 4.4, about 1 ps after the laser pulse, phonon heating effects become dominant for reducing the cooling rates.

The time evolving LO phonon distribution function N(q) is calculated in terms of the phonon wavevector q and assumed to be isotropic in q. Figures 4.5~8 trace the non-equilibrium LO phonon populations evolving with time. At 77 $^{\circ}$K, the value of the equilibrium phonon distribution is about 4.179×10^{-3}, as indicated by the arrow in Fig. 4.5. It is known that the strongly perturbed phonon distribution is due solely to the strong LO-phonon emission of the hot electrons. After the excitation, reabsorption of the emitted phonons by the carriers and the phonon-phonon losses bring the distribution back to the equilibrium value. It is noted that even a few picoseconds after the laser pulse, a significant number of phonons still exist, and a considerable number of phonon reabsorptions still go on. Since the numbers of electrons and holes residing in the ensemble being simulated are taken to be as small as 2000 respectively in order to save the computer time, the crude approximation results in the jumps of the phonon distribution functions, as shown in Figs. 4.5~8, which are expected to be smooth curves. The disturbances of other types of phonons are ignored in this calculation. Actually, emission of TO phonons, which only couple to the holes, also provides a contribution to the energy loss[16].

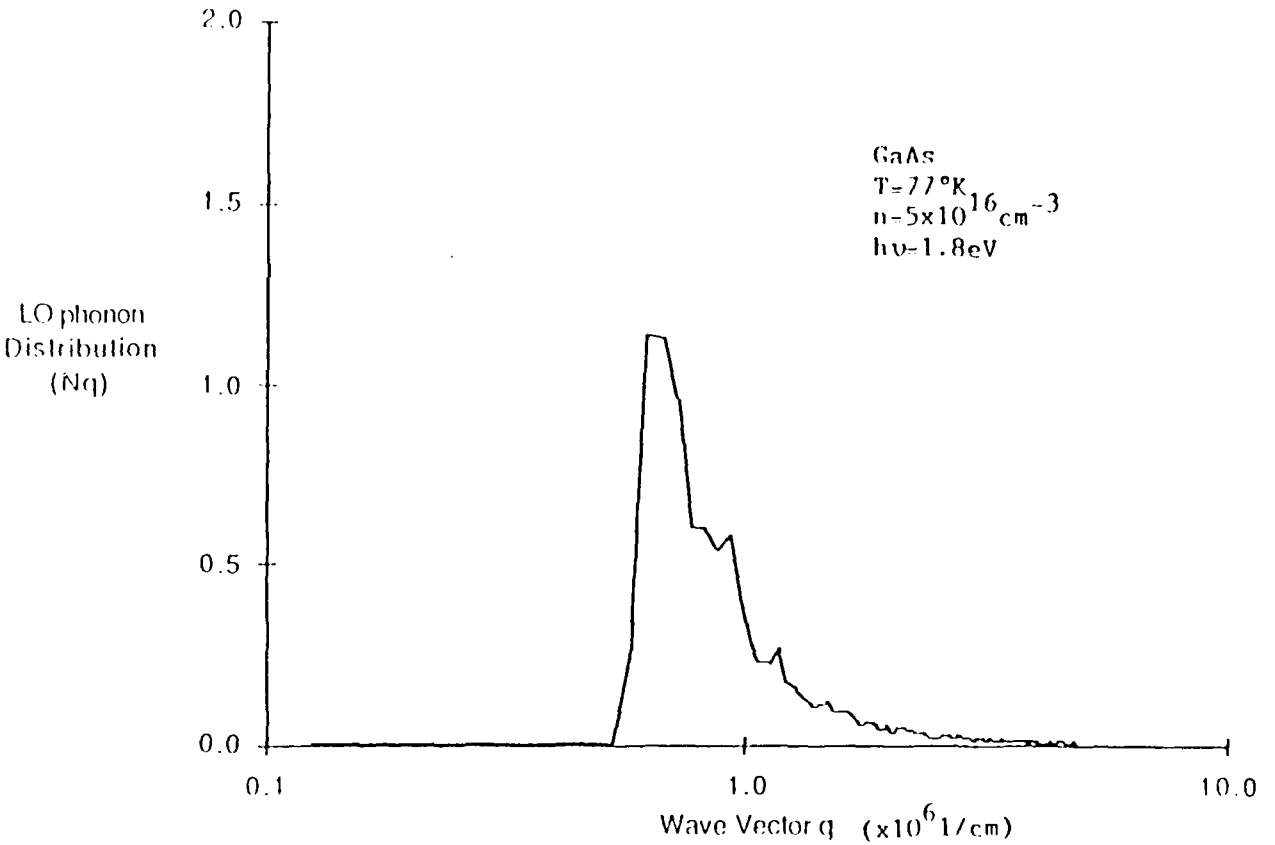

Fig. 4.5 The non-equilibrium LO phonon occupation number versus phonon wave vector q at t=0.2 ps.

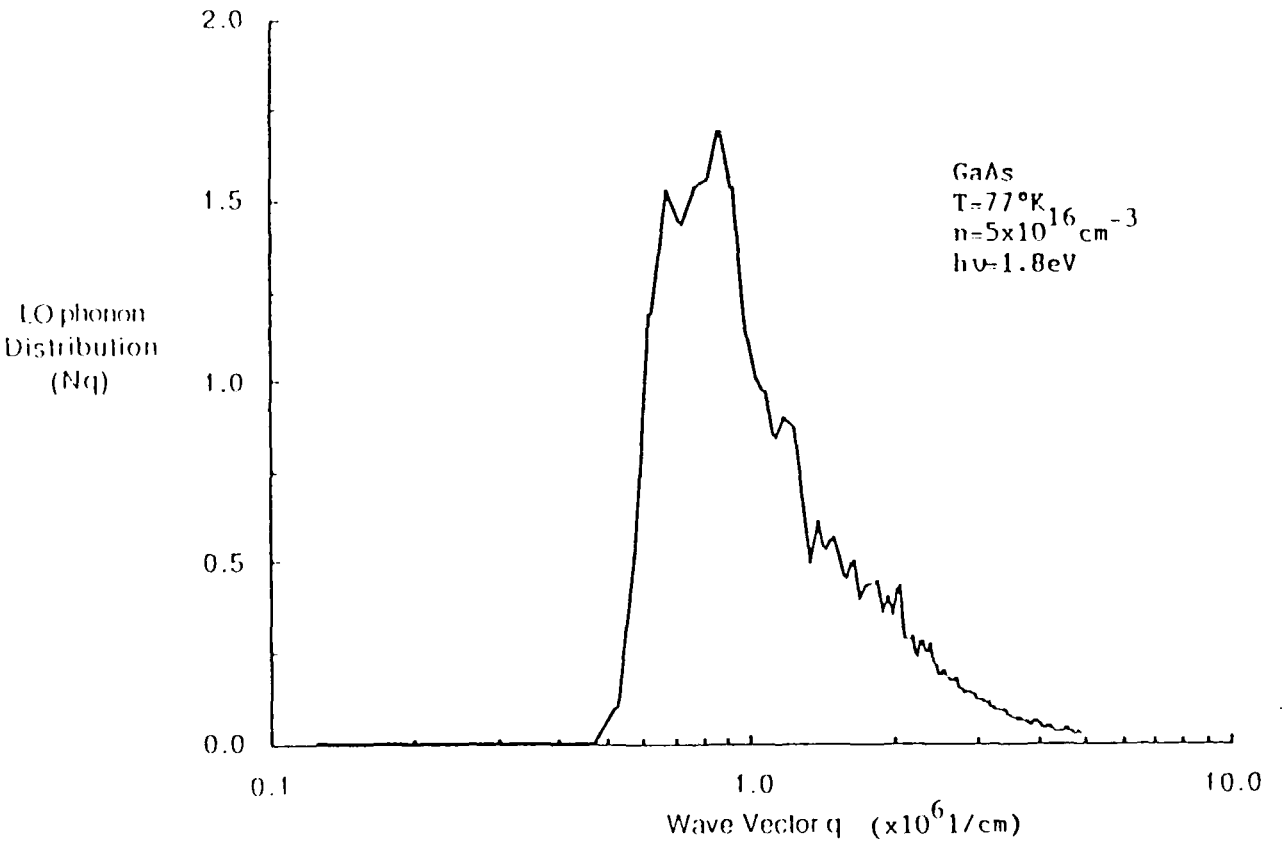

Fig. 4.6 The non-equilibrium LO phonon occupation number versus phonon wave vector q at t=2 ps.

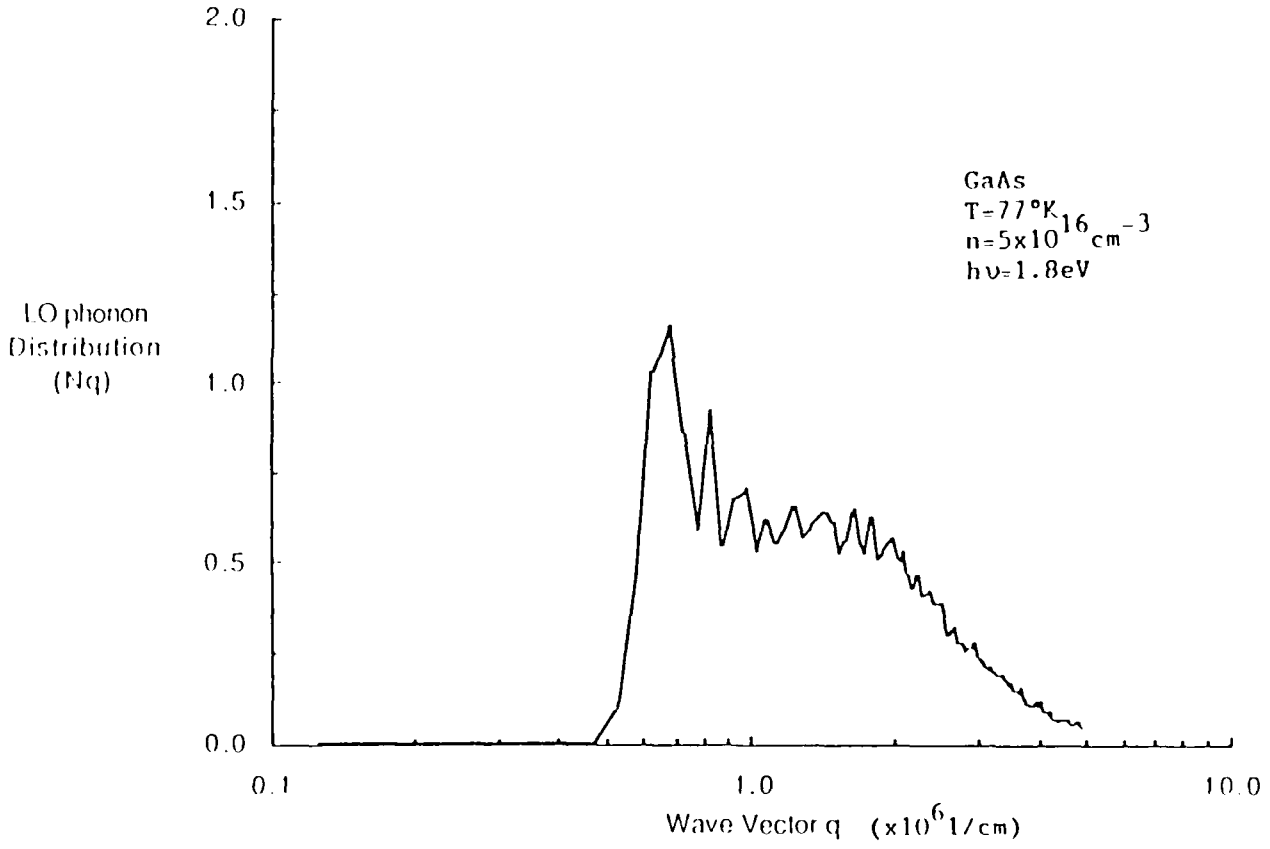

Fig. 4.7 The non-equilibrium LO Phonon occupation number versus phonon wave vector q at t=5 ps.

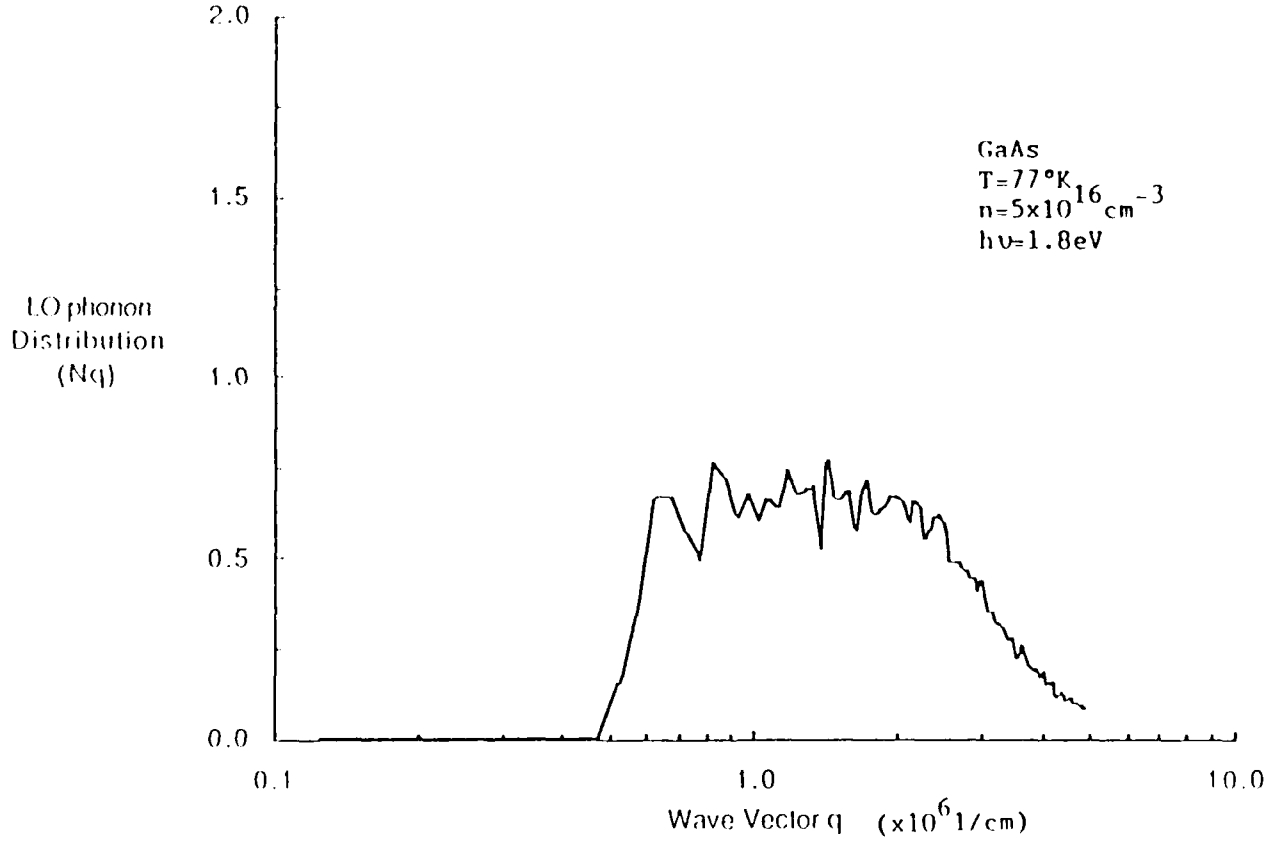

Fig. 4.8 The non equilibrium LO phonon occupation number versus phonon wave vector q at t-10 ps.

As expected, hot phonon effects are mainly responsible for the relatively high carrier temperatures observed in experiments investigated in the subpicosecond time regime. The deviation of the phonon population from its equilibrium value further slows down the hot electron relaxation, which bring closer agreement between theoretical and experimental results for laser-excited GaAs.

4.3 Screening Effect of Electron-Phonon Interaction

Free carrier screening reduces the cooling rates, but not sufficiently to explain the experimental data. It is noted that inclusion of hot phonon effects leads to closer agreement between experiment and theory. In this section, the cooling rates of the laser-excited electrons were calculated in the absence of the carrier-carrier interactions, hot phonon effects and in the presence of holes using both the Debye-Hückel and the self-consistent screening models to better demonstrate the screening effcet.

Figure 4.9 illustrates that the screening effect reduces the cooling rates, as compared to the case where screening is ignored. The lowest curve represents the cooling rate when screening is totally ignored, which is too fast compared to the observed slow cooling rates at high excitation levels. When the screening of the electron-phonon interaction is considered, the cooling rate is reduced to a different extent through the two different screening models. In the self-consistent screening model, the screening evolves as the carriers relax and the screening length is calculated self-consistently as

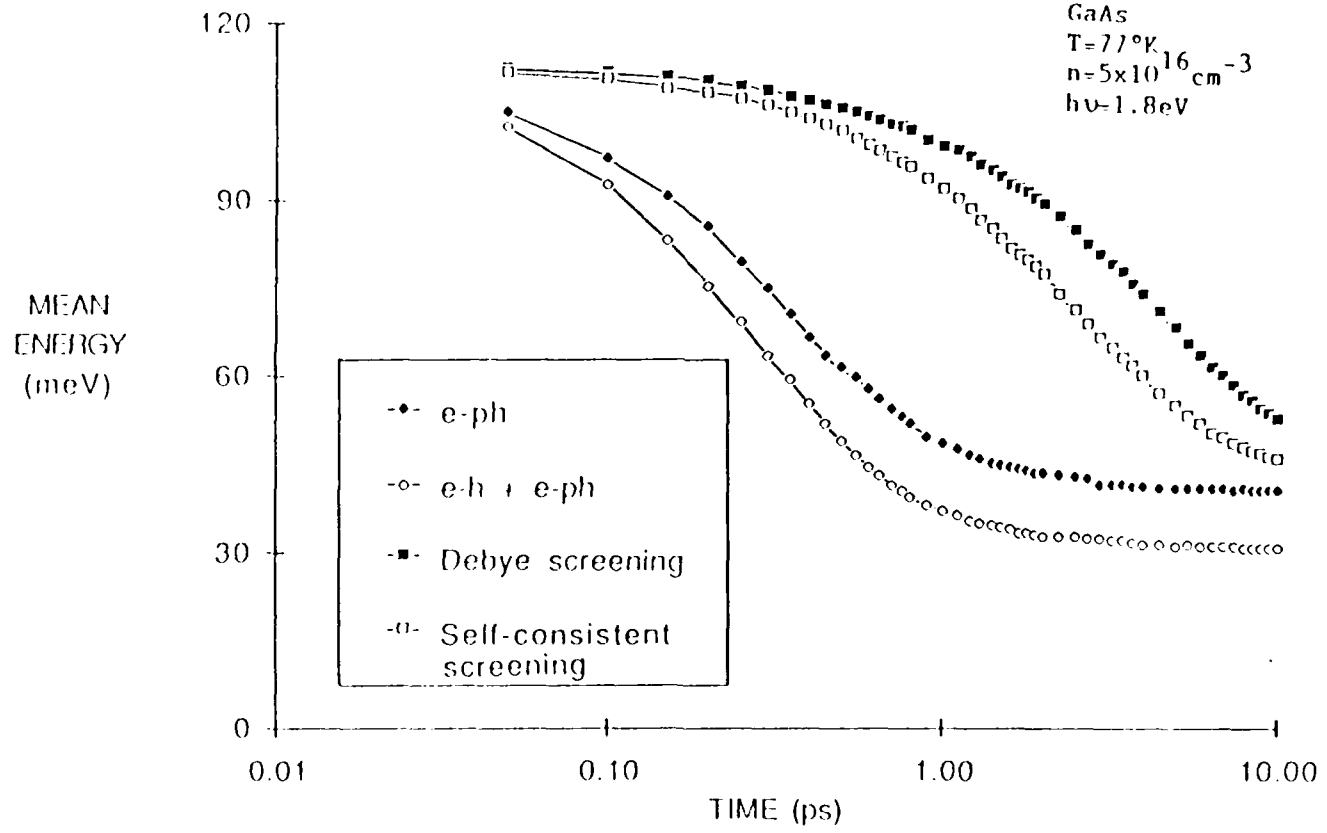

Fig. 4.9 The time evolution of electron mean energies for different screening models of the electron-phonon interactions: 1) e-ph (Debye screening), 2) e-ph (self-consistent screening), 3) e-ph (no screening), and 4) e-ph and e-h (no screening).

discussed in Sec. 3.3.2. The reduction of the cooling rate is smaller for the self-consistent model, which gives more reasonable estimates of the screening length and reflects the time evolution of the carrier distribution functions. The Debye-Hückel model overestimates the screening due to the equilibrium Boltzmann distribution function imposed on the carriers.

4.4 Time Evolution of Electron Energy Distribution Function

In this section, the manner in which the electron-hole and carrier-phonon interactions affect the form of the energy distribution function of hot electrons is examined. Figure 4.10 illustrates the distribution function of electrons at 0.25 ps after a 1.8 ev, delta-shaped laser pulse at an excitation level of $5x10^{16}cm^{-3}$. This figure displays peaks below the initial energy, displaced at integral multiples of the LO phonon emission threshold (about 36.4 mev). Even at 1 ps after the laser pulse, the distribution function still shows some peaks, as depicted in Fig. 4.11, which assures us that the electrons cascade down to lower energies mainly by emitting LO phonons. It is shown that the electron-phonon interaction dominates the cooling at low excitation levels. The peaks are broadened by the electron-hole scatterings and it seems that there are more electrons on the lower side of the peaks, indicating the energy loss by the electrons during the electron-hole scatterings. Figure 4.12 illustrates the distribution function at 5 ps, which seems becoming a

Fermi-like distribution. The electrons have already lost most of their energy at this stage.

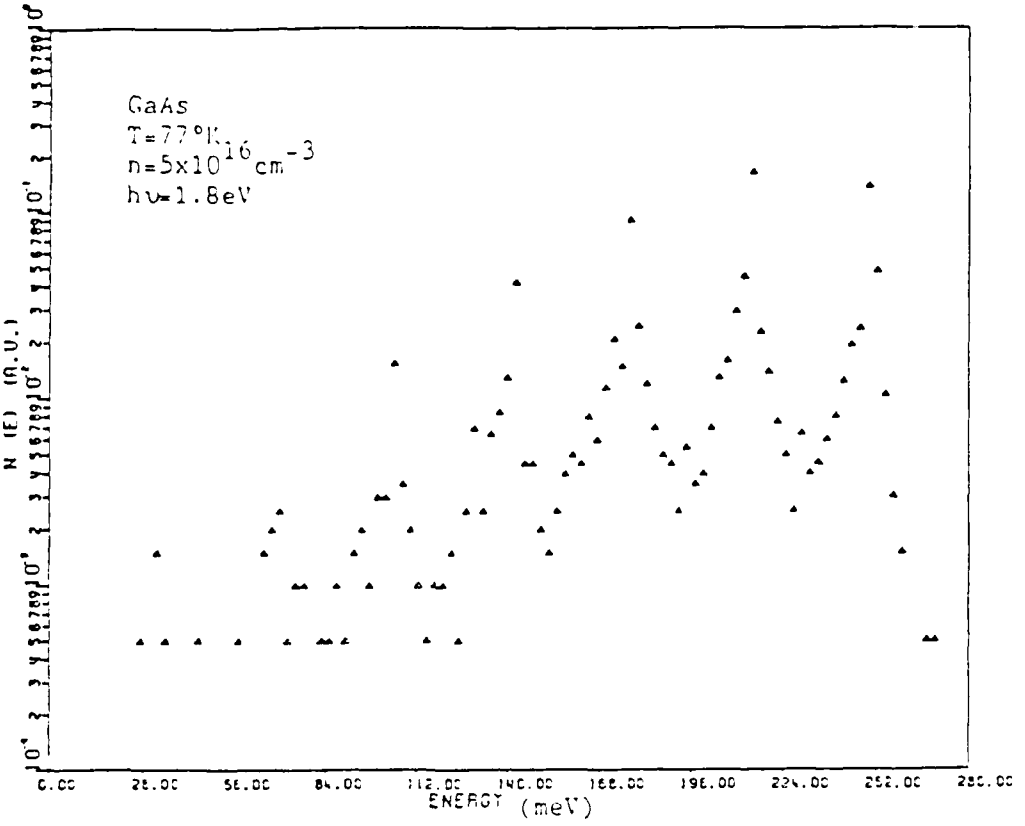

Fig. 4.10 The electron energy distribution function at 0.25 ps after the initial laser pulse, with e-ph and e-h interactions.

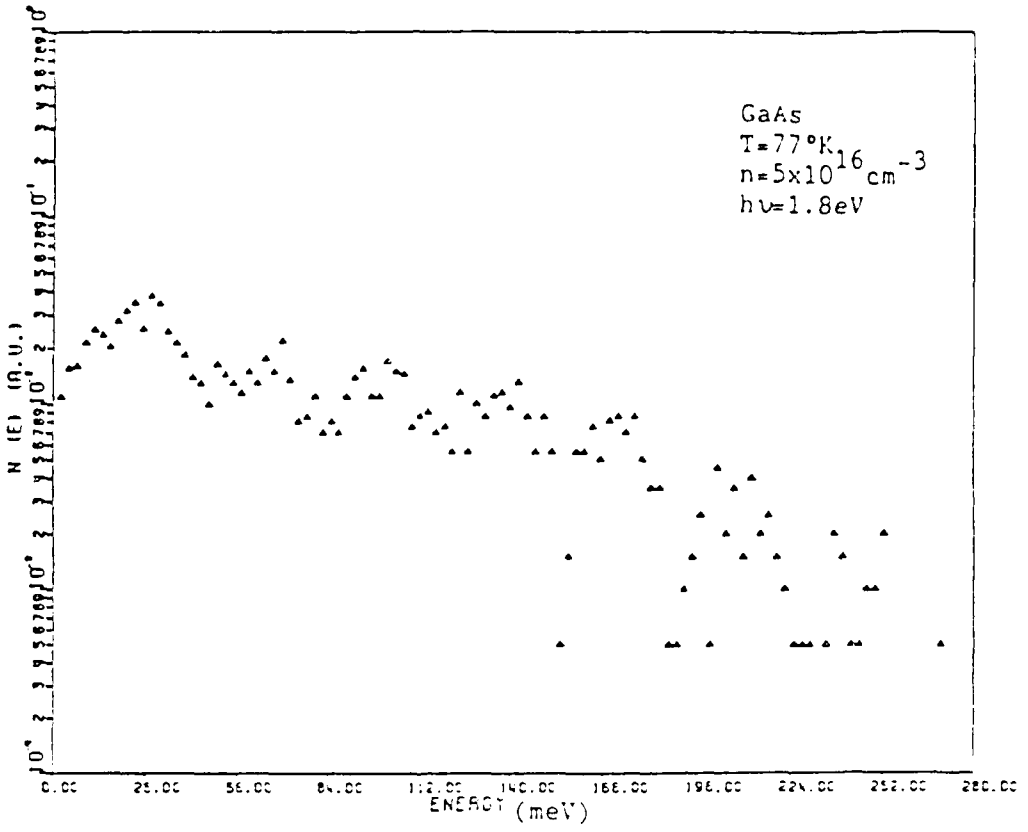

Fig. 4.11 The electron energy distribution function at 1 ps after the initial laser pulse, with e-ph and e-h interactions.

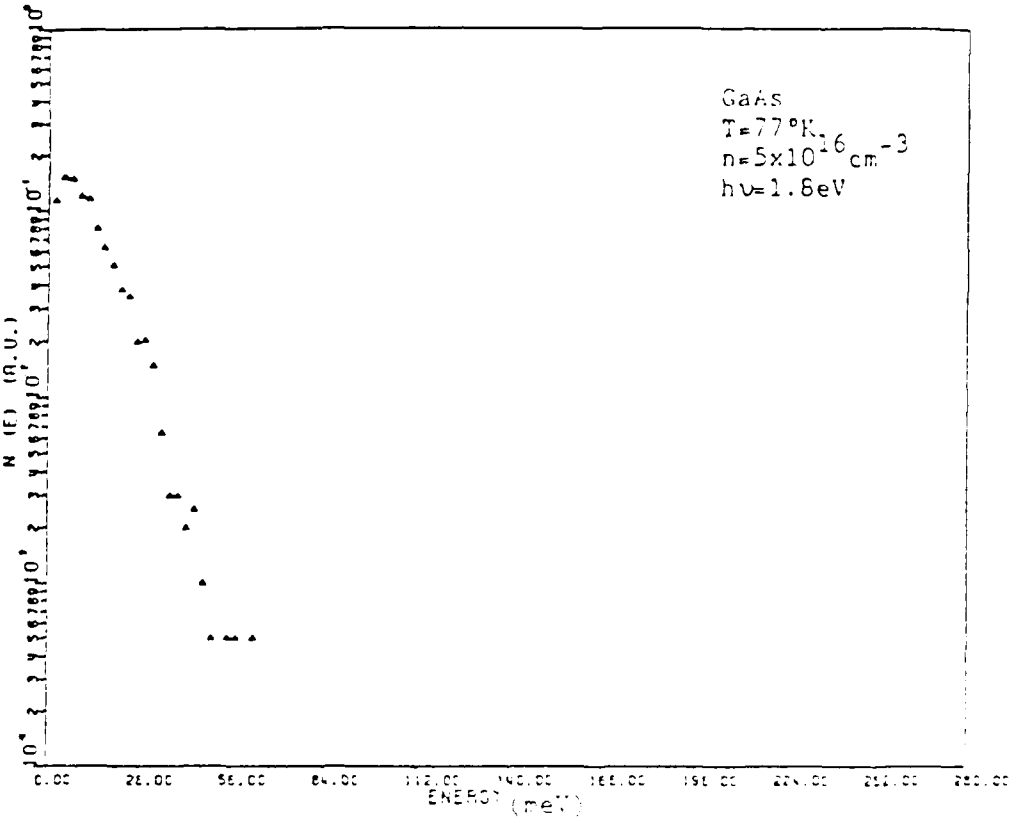

Fig. 4.12 The electron energy distribution function at 5 ps after the initial laser pulse, with e-ph and e-e interactions.

CHAPTER 5

CONCLUSIONS

The ensemble Monte Carlo technique provides very accurate microscopic information about the physical system under simulation and it does not require any assumption on the carrier distribution function because of the self-consistent time-evolving distribution function inherent within it. Additionally, using a more realistic band structure and a direct evaluation of the scattering probabilities for the various scattering mechanisms involved in the relaxation process becomes attainable.

The major purpose of this thesis is to develop an ensemble Monte Carlo method to simulate the hot laser-excited electron-hole system in bulk GaAs, taking account of the carrier-phonon interaction, electron-hole interaction, and hot phonon effects in order to obtain closer agreement between the theoretically calculated and experimentally observed cooling rates of hot photoexcited carriers in semiconductors. Generally, the relaxation of hot laser-excited carriers can be divided into three stages. The first stage is the very fast initial relaxation where the carriers lose most of their excess energy. In the second stage, the hot distribution cools towards the lattice temperature until the optical phonons are no longer able to remove energy. The first two stages take typically over within 100 ps. The third stage occurs in the nanosecond time region involving the final cooling of the distribution to the lattice temperature through the acoustic phonon emission.

It is known that the electron-phonon interaction is the dominant channel for energy loss by hot electrons at low excitation levels, while at high excitation levels, the electron-hole interaction is the main channel. The holes then dissipate energy through the hole-phonon interaction via the unscreened TO phonon deformation potential interaction. The electron-hole interaction promotes the cooling rate of hot electrons at high carrier densities by channeling the electron energy to the holes and then to the lattice. However, it slows down the cooling rate at low carrier densities due to the shifting of the electron population to energies below the LO phonon emission threshold. The cooling rate has been found to decrease with increasing excitation level because both hot phonon effects and screening become more important in a high density plasma. If the carrier density is large enough, the optical phonons will be reabsorbed before they start to decay. The experimentally observed high kinetic energy of the electron-hole plasma is shown to be mainly due to LO phonon heating which provides the dominant mechanism to explain the slowing down of the cooling rate as well as the thermalization of the electrons and holes.

Recently, there has been an extensively interest in the two dimensional quantum well structure. The behavior of the electrons in quantum well differ drastically from the three dimensional bulk semiconductors. A further understanding of carrier cooling in quantum well structures requires more detailed knowledge of the phonons in these systems. Extending the present work to two dimensional quantum well structures will be an exciting task to carry on in the near

future to understand the ultrafast relaxation mechanisms of the hot photoexcited carriers inside the quantum well.

REFERENCES

[1] C.L. Tang, F.W. Wise, and M.J. Rosker, 18th International Conference on Solid State Devices and Materials, Tokyo, p. 157-159, 1986.

[2] R.B. Hammond, Physica vol. 134B, p. 475, 1985.

[3] C.V. Shank, R.L. Fork, B.I. Greene, F.K. Reinhart, and R.A. Logan, Appl. Phys. Lett. vol. 38, p. 104, 1981.

[4] Z.Y. Xu and C.L. Tang, Appl. Phys. Lett. vol. 44, p. 692, 1984.

[5] K. Kash and J. Shah, J. Lumin. vol. 30, p. 333, 1985.

[6] D. von der Linde, J. Kuhl, and H. Klingenberg, Phys. Rev. Lett. vol. 44, p. 1505, 1980.

[7] J.C. Tsang, J.A. Kash, and S.S. Jha, Physica vol. 134B, p. 184, 1985.

[8] J.A. Kash, J.C. Tsang, and J.M. Hvam, Phys. Rev. Lett. vol. 54, p. 2151, 1985.

[9] C.L. Collins and Y. Yu, Sol. State Commun. vol. 51, p. 123, 1984.

[10] L.C. Allen, Phys. Rev. vol. 98, p. 993, 1955.

[11] A.R. Vasconcellos and R. Luzzi, Sol. State Commun. vol. 49, p. 587, 1984.

[12] W. Fawcett, A.D. Boardman, and S. Swain, J. Phys. Chem. Solids vol. 31, p. 1963, 1970.

[13] R.F. Leheny, J. Shah, R.L. Fork, C.V. Shank, and A. Migus, Sol. State Commun. vol. 31, p. 809, 1979.

[14] R.A. HOpfel, J. Shah, and A.C. Gossard, Phys. Rev. Lett. vol. 56, p. 765, 1986.

[15] M. Ashe and O.G. Sarbei, Phys. Stat. Sol.(b) vol. 126, p. 607, 1984.

[16] W. POtz and P. Kocevar, Phys. Rev. vol. 28B, p. 7040, 1983.

[17] E.J. Yoffa, Phys. Rev. vol. 23B, p. 1909, 1981.

[18] W. Grandszus and E.O. GObel, Physica vol. 117B & 118B, p. 555, 1983.

[19] W. Pötz, "Hot Phonon Effects in Bulk GaAs," to be published.

[20] Y.B. Levinson and B.N. Levinsky, Sol. State Commun. vol. 16, p. 713, 1975.

[21] M. Pugnet, J. Collet, and A. Cornet, Sol. State Commun. vol. 38, p. 531, 1981.

[22] R. Luzzi, J. Lumin. vol. 30, p. 318, 1985.

[23] P. Kocevar, Physica vol. 134B, p. 155, 1985.

[24] J. Collet and T. Amand, J. Phys. Chem. Solids vol. 47, p. 153, 1986.

[25] P. Lugli, C. Jacoboni, L. Reggiani, and P. Kocevar, Appl. Phys. Lett. vol. 50, no. 18, p. 1251, 1987.

[26] J.C. Phillips, Phys. Rev. vol. 112, p. 685, 1958.

[27] R.A. Smith, "Semiconductors," 2nd edition, Cambridge University Press, London, 1979.

[28] J.R. Chelikowsky and M.L. Cohen, Phys. Rev. vol. 14B, p. 556, 1976.

[29] M. Reine, R. Aggarwal, B. Lax, and C. Wolfe, Phys. Rev. vol. 2B, p. 458, 1970.

[30] R.D. Dupuis, P.D. Dapkus, R.M. Kolbas, and N. Holonyak, Sol. State Commun. vol. 27, p. 531, 1978.

[31] B.P. Zakharchenya, D.N. Mirlin, V.I. Perel, and I.I. Reshina, Usp. Fiz. Nauk vol. 136, p. 459, 1982 [Sov. Phys. Usp. vol. 25, p. 143, 1982].

[32] D.E. Aspnes, Phys. Rev. vol. 14B, p. 5331, 1976.

[33] O. Madelung, in "Physics of Group IV Elements and III-V Compounds," vol. 17a of "Landolt-Bornstein," edited by K.H. Hellwege (Springer, Berlin, 1981).

[34] A.J. Taylor, D.J. Erskine, and C.L. Tang, Opt. Soc. Am. vol. 2B, p. 663, 1985.

[35] C. Jacoboni and L. Reggiani, Review of Modern Physics vol. 55, no. 3, p. 645, 1983.

[36] M. Osman, Ph.D. dissertation, Arizona State University, Summer 1986.

[37] C. Jacoboni and L. Reggiani, Advances in Physics vol. 28, no. 4, p. 493-553, 1979.

[38] A.J.C. Sampaio and R. Luzzi, J. Phys. Chem. Solids vol. 44, no. 6, p. 479-488, 1983.

[39] J. Shah, J. Phys. (Paris), Colloq. 42, C7-445, 1981.

[40] C.L. Tang and D.J. Erskine, Phys. Rev. Lett. vol. 51, p. 840, 1983.

[41] D.J. Erskine, A.J. Taylor, and C.L. Tang, Appl. Phys. Lett. vol. 45, p. 54, 1984.

[42] A.J. Taylor, D.J. Erskine, and C.L. Tang, Appl. Phys. Lett. vol. 43, p. 989, 1983.

[43] J.L. Oudar, I. Abram, A. Migus, D. Hulin, G. Grillon, and J. Etchepare, J. Lumin. vol. 30, p. 340, 1984.

[44] J.L. Oudar, A. Migus, D. Hulin, G. Grillon, J. Etchepare, and N. Antonetti, Phys. Rev. Lett. vol. 53, p. 384, 1984.

[45] S.A. Lyon, J. Lumin. vol. 35, p. 121-154, 1986.

[46] C.L. Collins and P.Y. Yi, Phys. Rev. vol. 30B, p. 4501, 1984. Physica vol. 117B & 118B, p. 386, 1983.

[47] P. Lugli, Ph.D. dissertation, Colorado State University, 1985.

[48] J.D. Wiley, Phys. Rev. vol. 4B, p. 2485, 1971.

[49] E. Conwell, "High Field Transport in Semiconductors," Solid State Physics, Suppl. 9 (Academic, New York), 1967.

[50] W.A. Harrison, Phys. Rev. vol. 104, p. 1281, 1956.

[51] P. Lugli and D.K. Ferry, Physica vol. 117B, p. 251, 1983.

[52] M. Costato and L. Reggiani, Phys. Status Solidi vol.58B, p. 471, 1973.

[53] K. Brennan and K. Hess, Phys. Rev. vol. 29B, p. 5581, 1984.

[54] H.D. Rees, J. Phys. Chem. Solids vol. 30, p. 643, 1969.

[55] M.A. Osman, W. Pötz, and D.K. Ferry, "Self-Consistent Screening Length Calculation Using EMC Method." unpublished.

[56] N. Takenaka, M.Inoue, and Y. Inuishi, J. Phys. Soc. Jpn. vol. 47, p. 861, 1979.

[57] M.A. Osman, H.L. Grubin, P. Lugli, M.J. Kann, and D.K. Ferry, "Monte Carlo Investigation of Hot Photoexcited Electron Relaxation in GaAs," 2nd Topical Meeting on Picosecond Electronics and Optoelectronics, Jan. 1987, Lake Tahoe, Nevada.

[58] D.K. Ferry, M.A. Osman, R. Joshi, and M.J. Kann, "Ultrafast Relaxation of Hot Photoexcited Carriers in GaAs," the 5th International Conference on Hot Carriers in Semiconductors, Boston, July 20-24, 1987.

END

FILMED

MARCH, 1988

DTIC